THE APPLICATION OF MICROWAVE LENSES TO ANTENNA MEASUREMENTS

by

Thomas H. Legg

A thesis submitted to the Faculty of Graduate Studies and Research, McGill University, in partial fulfilment of the requirements for the degree of Master of Science.

Eaton Electronics Research Laboratory
McGill University, Montreal

April, 1956.

TABLE OF CONTENTS

SUMMARY

Laboratory methods of measuring the radiation characteristics of microwave antennas were investigated at a wavelength of 1.25 cm. The methods consisted of rotating the antenna in question in a microwave beam issuing from a collimating lens made from polystyrene plastic. With uniform illumination of the lens, diffraction from its edge caused severe departure of the beam from the plane wave desired for antenna measurements; inaccuracies in the measured antenna characteristics resulted. Techniques to reduce the effects of diffraction are described. In each case considered, the amplitude and phase variations across the beam were measured. The results show that by illuminating a lens non uniformly in a special manner, diffraction effects can be reduced, and antenna patterns measured with accuracy.

Lastly, a method of measuring radiation patterns by rotating the antenna and lens as a whole is described. This method is applicable to special antennas; it was also found suitable in measuring the scattering characteristics of certain types of bodies.

Acknowledgements

The author is indebted to Dr. G. Bekefi who suggested the research topic and directed the work involved in this thesis. In numerous discussions with Dr. Bekefi, new ideas were often formed, and invariably problems were clarified. Much assistance in the construction of apparatus was given by Mr. V. Avarlaid and his staff.

During part of the time spent on this research, generous financial aid was received from the Defence Research Board, Ottawa, Ontario; in addition, some of the equipment used in the work was bought on a grant given by the Defence Research Board on contract: DRB 9512-20. The research forms part of a project on Microwave Optics supported at McGill University by the United States Air Force, Cambridge Research Center, Cambridge, Mass. on contract: AF-19(122)-81.

Chapter I.

INTRODUCTION.

The object of the research described in this thesis is twofold: first, to produce in a laboratory a microwave beam departing as little as possible from a plane wave; secondly, to use this plane wave in measurements of the radiation characteristics of antennas or scattering objects.

The need for a plane wave field arises from the fact that the radiation characteristics of antennas are expressed in terms of their response to such a plane wave, as function of the antenna's orientation in the field. Moreover, the characteristics of scattering objects are studied by measuring the energy scattered in various directions when an object is immersed in a beam of plane waves.

By a plane wave field is meant one that is uniform in both amplitude and phase over the antenna or scatterer in question. This requirement can be met to within a good degree of approximation by removing the antenna or scatterer under test sufficiently far from the radiating source. A sketch of the arrangement is shown in figure (1.1). Noted on the figure are criteria derived by silver[1] for the separation (R) that is needed in order that the phase over the aperture of the antenna being investigated does not vary by more than about 20 degrees, and the intensity by not more than 10%. Although these criteria are chosen somewhat arbitrarily, it is found

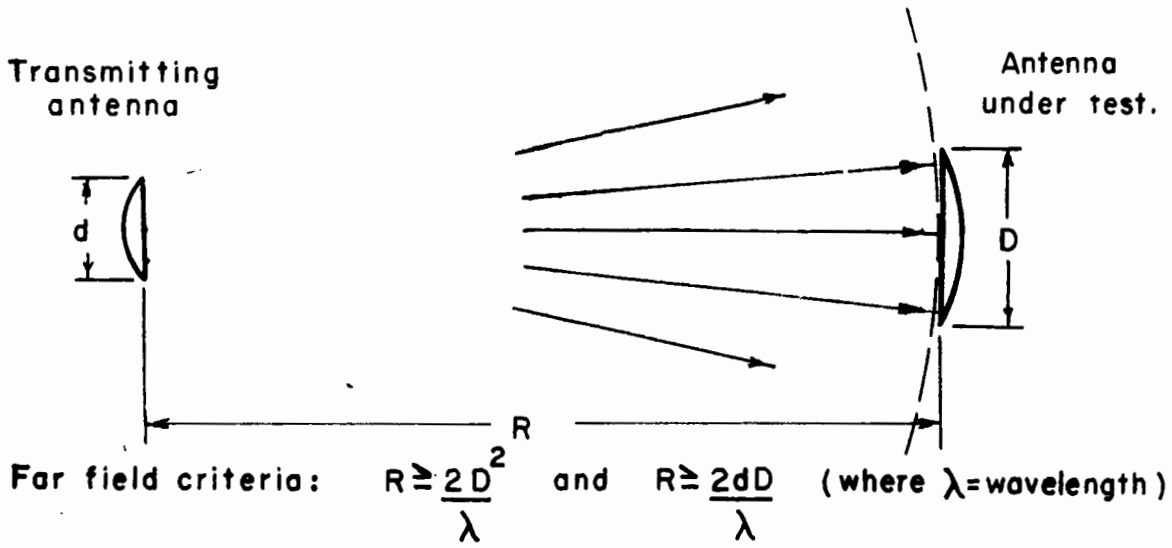

Fig. 1.1: The arrangement for far field antenna measurements, showing the criteria for separation (R).

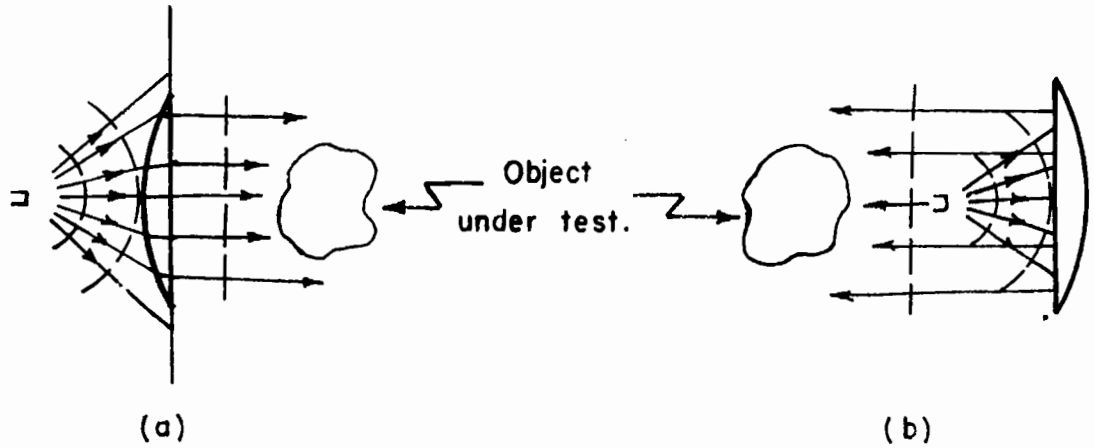

Fig. 1.2: Indoor methods of antenna or scatterer measurements based on geometrical optics principles: (a) Collimation with a lens, (b) Collimation with a parabolic reflector.

that when they are satisfied, the measured radiation characteristics differ very little from the true characteristics that would be measured with a perfect plane wave.

Because the distance (R) required between the source and the antenna under test can become extremely large, outdoor sites are generally essential for this method of measurement. Such sites must be free from intervening buildings and other obstacles and are often not available. Apart from these objections, weather conditions frequently prevent accurate measurements from being made. This is particularly true in scattering measurements, where it is found that, because of the way that the scatterers must be supported, even small wind disturbances preclude meaningful observations entirely. Further, with a large distance separating the transmitter from the antenna or scatterer to be investigated, adjustments are inconvenient, and seldom is the accuracy or flexibility of adjustment attained that could be achieved indoors.

Clearly then, a laboratory method of measuring antenna or scatterer characteristics is desirable. Some investigations have been undertaken in the past with this view in mind. The fundamental idea in all the work that has been done so far, concerns the use of a lens or reflector as a collimating device. The methods used, based upon geometrical optics principles, are depicted schematically in figure (1.2). Woonton, Borts, and Carruthers,[2] used a rectangular metal plate lens to collimate the energy issuing from a small source, and investigated the radiation characteristics of electromagnetic

horns in the field. Crysdale's[3] work differed from the above only insofar that a parabaloidal reflector was used in place of the metal plate lens. Hogg[4] employed a rotationally symmetric plastic lens as a collimator and studied the scattering properties of plates and wires.

The investigations summarized above were on the whole fairly successful. It was realized by the workers mentioned that the major limitation in accuracy was imposed by diffraction effects arising from the finite size of the collimating devices, which in general do not measure more than one hundred wavelengths. With this realization, Woonton, Carruthers, Elliot and Rigby,[5] and McCormick,[6] made careful theoretical and experimental investigations of these diffraction effects and the errors which they cause in antenna measurements.

The work described in this thesis deals with methods leading to a better approximation of a plane wave field than that obtained using the simple optical analogies depicted in figure (1.2). The basic idea rests upon the effective reduction of diffraction from the rim of the collimating system, by decreasing the energy of the incident field towards the edge of the collimator in question. This was found to provide great improvement in the amplitude distribution of the emerging wave, but led to some deterioration in the phase distribution. The latter defect was overcome by a simultaneous adjustment of not only the amplitude, but also the phase of the wave incident upon the collimator.

To give a realistic evaluation of the usefulness of the various beams produced, the radiation patterns of several electromagnetic horns were measured in these beams. Considerable improvement over the earlier attempts was found.

Chapter 2.

STUDY OF MICROWAVE COLLIMATING SYSTEMS AND LABORATORY INVESTIGATIONS OF THE RADIATION PATTERNS OF MICROWAVE HORNS

In view of the fact that electromagnetic horns will be used as the test antennas in evaluating the quality of various collimating systems, these horns together with their radiation characteristics will be described first, before proceeding with a discussion of the collimating devices themselves.

The antennas that were used for this purpose were three electromagnetic horns of square aperture 10, 15 and 26 wavelengths to the side. (All experimental work was done at a wavelength of 1.235 cm.) These horns are described in Table I. Their radiation patterns were measured using the standard far field method as outlined in the introduction and in figure 1.1. A detailed description of the experimental arrangement will be found in Chapter 4.

The far field patterns of the three horns are shown in figure 2.1. The measurements were made in two planes of polarization known as the E and H-planes. The former refers to a rotation of the horn in the plane of the electric field, the latter, in the plane of the magnetic field. In these graphs, the ordinate represents the intensity on a decibel scale and the abscissa the angle of rotation of the horn relative to the direction of propogation of the plane wave.

In order to demonstrate the effect on the radiation

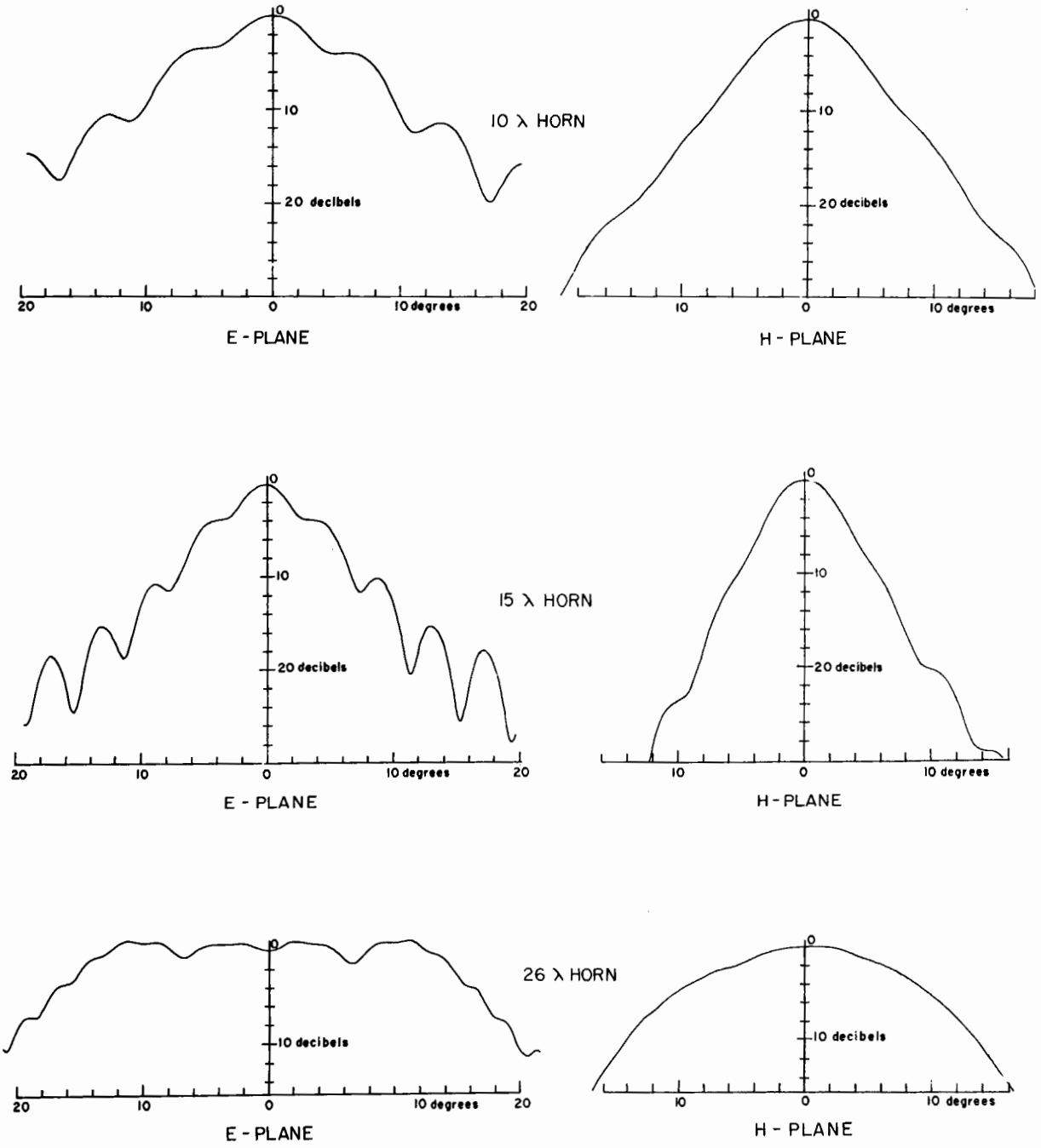

Fig. 2.1 : The far field patterns of three electromagnetic horns.

patterns when the criterion ($R \geq \frac{2D^2}{\lambda}$) for the distance (R) separating the transmitter from the receiver is not met, patterns for several horns were measured at various distances from a radiating point source (figure 2.2). The major error in the patterns results from the variation of phase over the mouth of the horns, while the amplitude distribution remains sensibly uniform. The phase error is due to the sphericity of the wave over the horn under test, and it can be easily demonstrated that this error is of magnitude:

$$\phi = \frac{kD^2}{8R} \text{ radians.}$$

where D is the linear size of the horn aperture, k is the wave number (2π/wavelength) and R is the separation between the horn and source.

It can be seen from figure 2.3 that reducing the distance R (and hence increasing the phase error ϕ) raises the level of the side lobes relative to the main lobe in the E-plane patterns and causes a broadening of the patterns themselves. Patterns measured in the H-plane showed mainly a broadening. The increase in side lobe level for the E-plane patterns of two horns (10λ and 15λ in size) is plotted in figure 2.4, as a function of the calculated phase error existing over the horn aperture. It is seen that the effects of phase variation over the antenna are striking; the results demonstrate the necessity of interposing a collimating system between the source and the antenna under test when laboratory measurements are contemplated.

TABLE I.

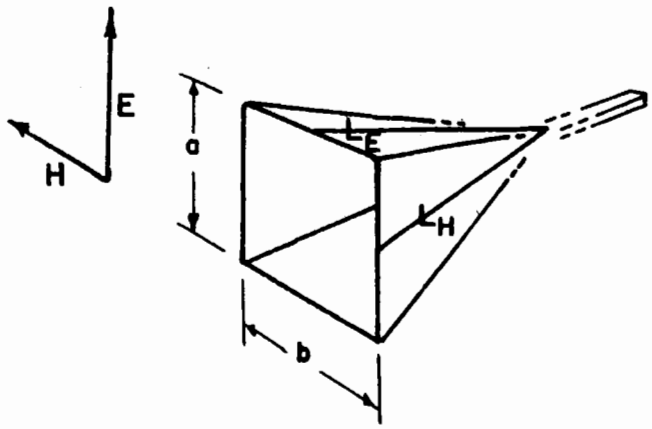

HORN	a	b	L_E	L_H
10λ	12.5	12.5	39.0	40.9
15λ	19.0	19.0	90.3	91.0
26λ	31.9	31.8	52.5	54.5

cms.

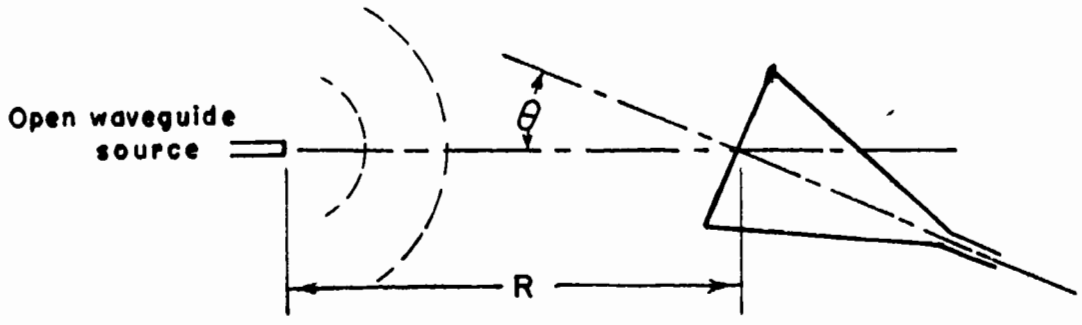

Fig. 2.2: The measurement of horn patterns using the spherical wave from an effective point source.

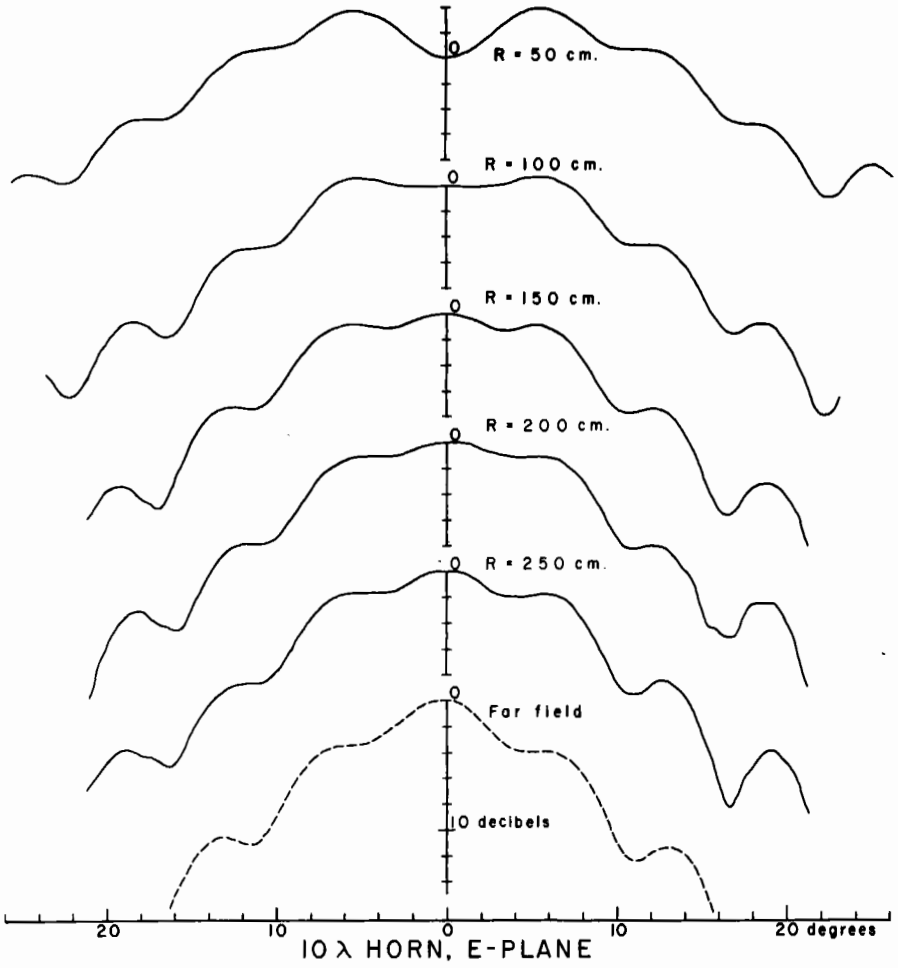

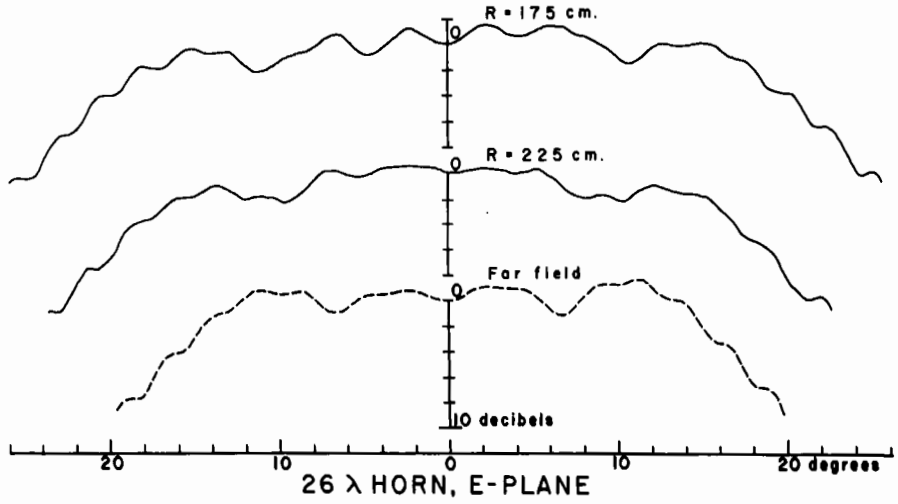

Fig. 2.3: The E-plane patterns of two horns measured at various distances (R) from an effective point source. The true far field patterns are shown in a dashed line for comparison.

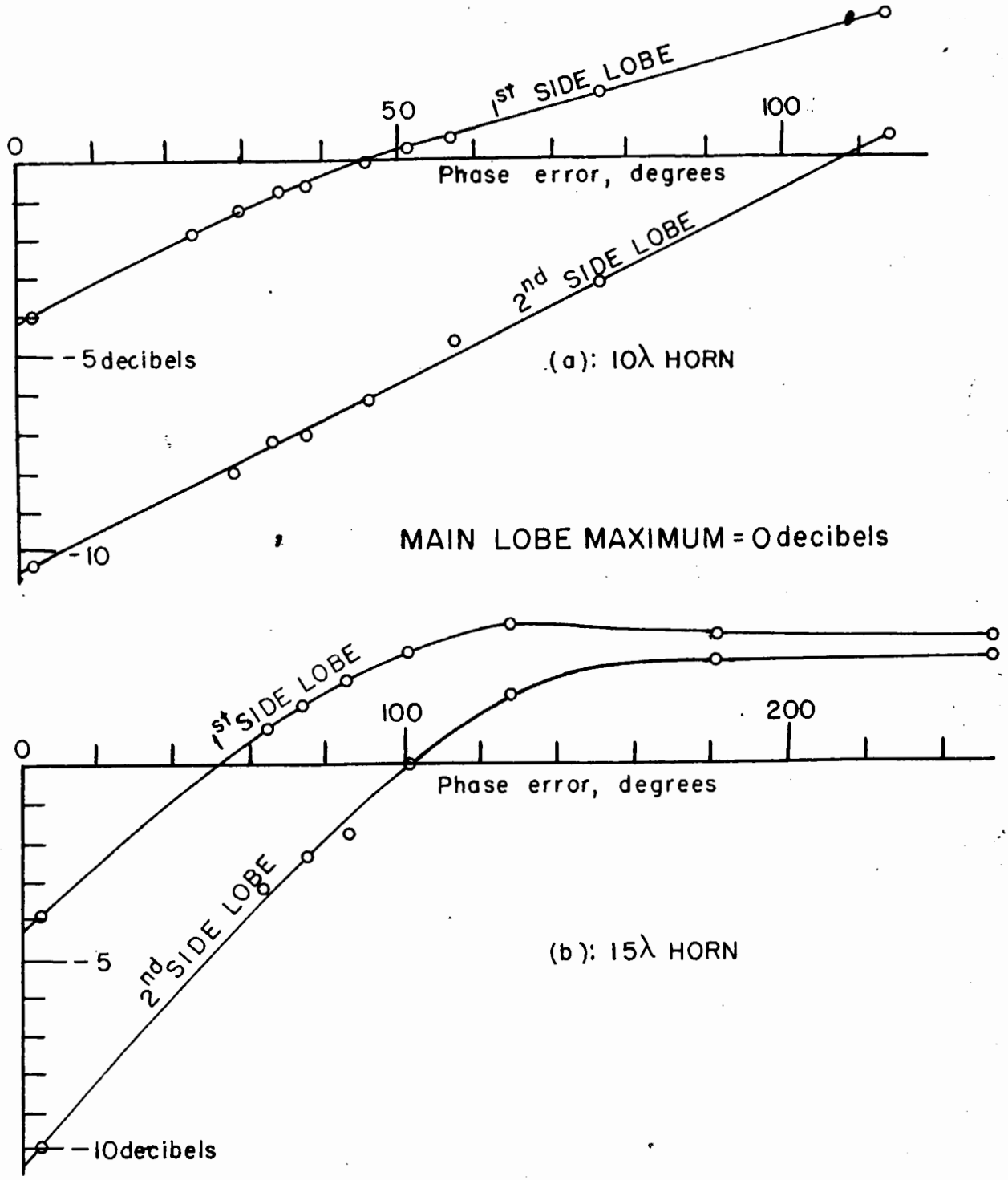

Fig. 2.4: The variation in first and second side lobe level in the E-plane patterns with respect to the main lobe, as function of the calculated phase error over the horn aperture.

The simplest type of collimating system has been described already in the introductory chapter. This system consists of a small source illuminating a lens or a paraboloidal reflector with a spherical wave of nearly constant amplitude. Before proceeding with more elaborate methods of illumination, a critical study will be made of this system (see figure 2.5) with a view to comparing and contrasting it with later modifications. Since frequent reference will be made to this arrangement it will be called System I for the sake of brevity.

2.1 The Collimating Properties of System I.

The optical arrangement shown in figure 2.5 consists of a lens (lens A described in Table II) mounted in a metal screen and illuminated by radiation from an open waveguide placed at the focus. The metal screen prevented any energy from reaching the image space by paths other than those through the lens itself, and the open waveguide acted as an effective point source of radiation. The diffraction from the rim of the lens, as mentioned previously, distorts what would otherwise be a plane wave beam. Although calculations of the field distribution could be made from the well known formula derived in Appendix I, the work is prohibitive and instead, measurements were made to demonstrate these diffraction effects.

TABLE II.

LENS	A	C	B
FOCAL LENGTH	250	100	50
DIAMETER	50	41.3	50
MATERIAL	SOLID POLYSTYRENE		
REFRACTIVE INDEX	1.579	1.585	1.579
DESCRIPTION	Corrected for spherical aberration with source at the focus. Plano-convex.	Corrected for spherical aberration and coma with source at the focus. Biconvex.	Corrected for spherical aberration and coma with source 100 cm. from lens surface. Biconvex.

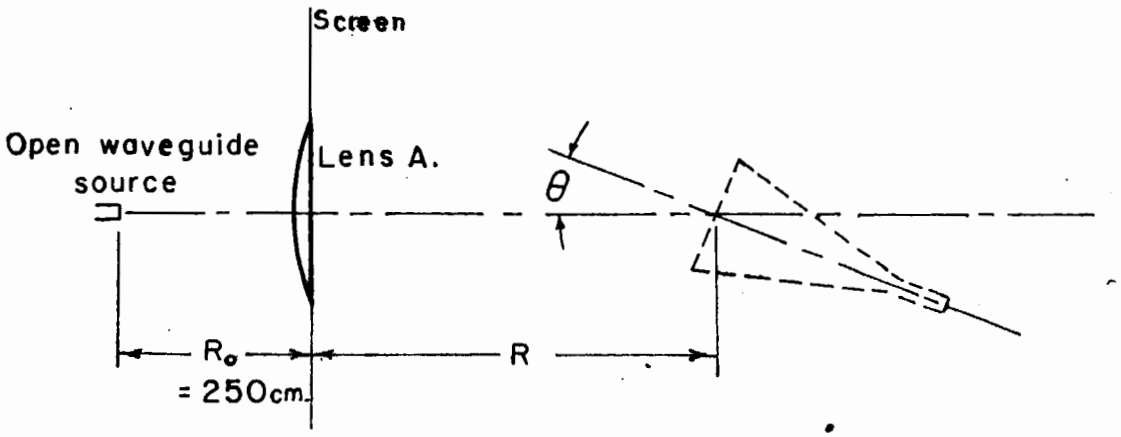

Fig. 2.5: System I: Uniform illumination of a collimating lens is provided by an effective point source placed at the focus. The position of an antenna when being tested is indicated with a dashed line.

Measurements of the field distribution were made at various distances from the lens in planes perpendicular to the optical axis. These scans of both the relative intensity and the relative phase are shown in figures 2.6 and 2.7 as functions of the distance of the measuring probe from the principal axis.

The fluctuations in intensity and phase (that is, the departure from a plane wave) are seen to be far greater than the tolerances of 10% (.5 decibels) intensity variation and 20 degrees phase variation allowable for antenna measurements. Furthermore, the field varies rapidly with distance from the lens, and this would suggest that any horn patterns measured in the field would be quite sensitive to the distance of the horn from the lens. This is borne out by measurements described below.

In passing, it should be noted that in a given plane, the intensity variations are much more drastic than the corresponding phase variations and moreover, that both the amplitude and phase become more nearly constant as the lens surface is approached. The latter observation forms the basis of some antenna and scatterer measurements described in Chapter 3.

Despite the poor characteristics of the field discussed when compared to a plane wave, horn patterns were nevertheless taken in this field with some hope that the horn may respond to the overall field and be insensitive to its finer details, particularly if the fluctuations are small but

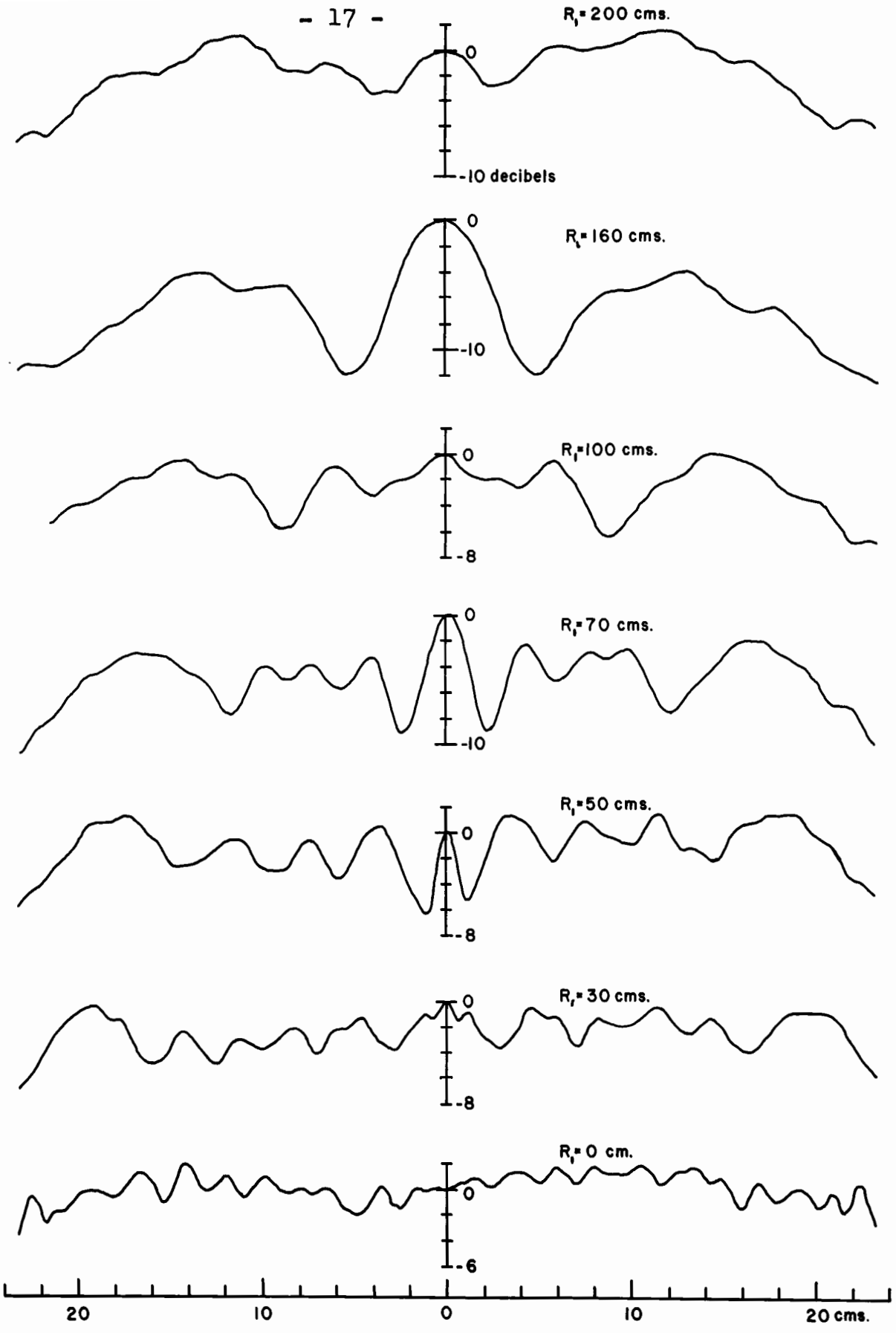

Fig. 2.6: Intensity scans (H-plane) in the collimated field of System I, at various distances (R_1) from the lens.

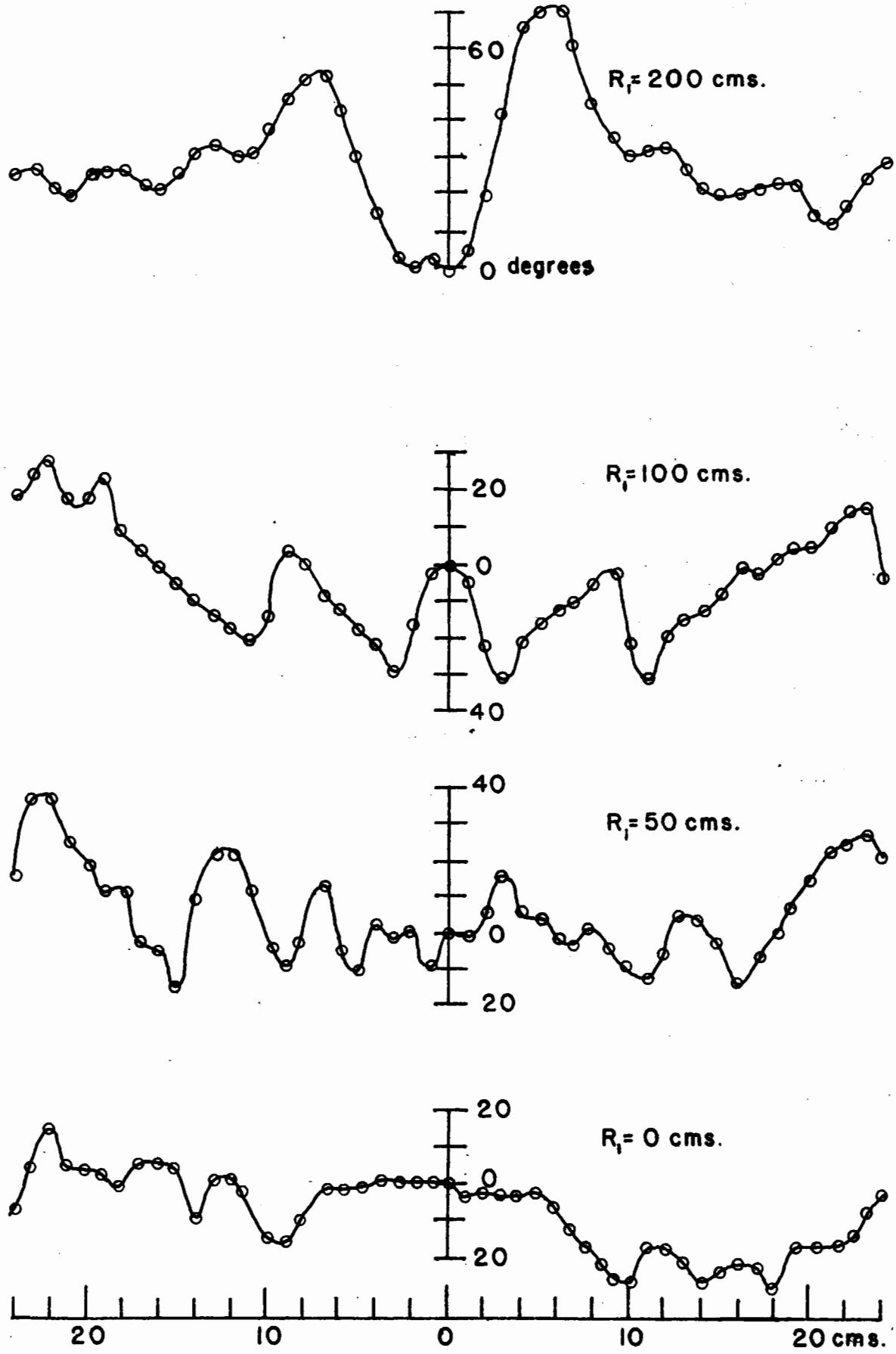

Fig. 2.7: Phase scans (H-plane) in the collimated field of System I.

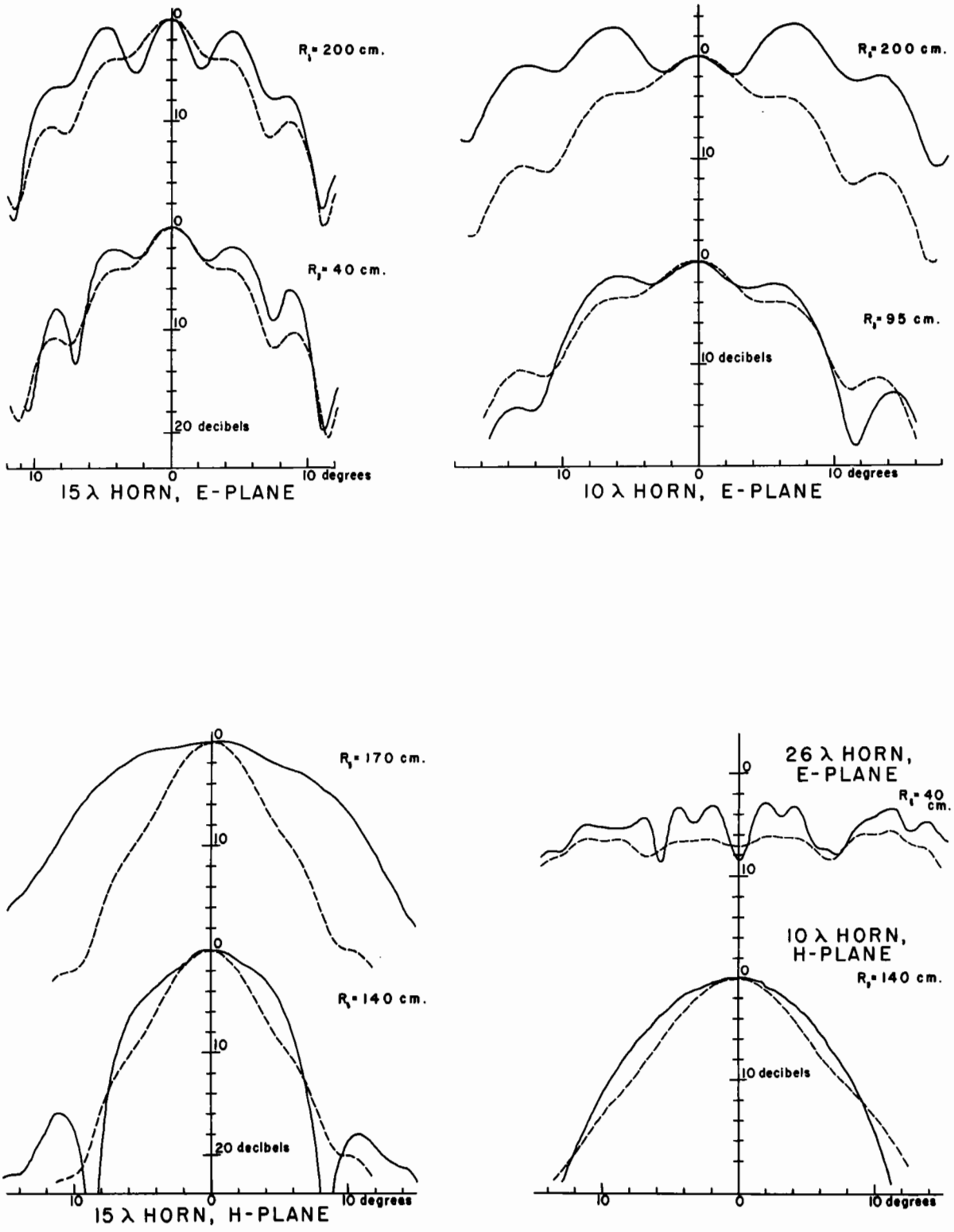

Fig. 2.8: Horn patterns measured at various distances (R_1) from the lens of System I. The true patterns are shown in a dashed line for comparison.

rapid. Although this effective smoothing out may take place to some extent, the horn patterns measured (see figure 2.8) indicate that the variations in amplitude and phase, are far too violent.

In figure 2.8, are shown the patterns of the three horns when measured at various distances (R_1) away from the lens. These results, traced in a solid line, are compared with the true far field patterns of the horns shown in a dotted line. It is seen that the departures from the true patterns far exceed what could in general be tolerated for accurate determinations of antenna characteristics. Not only do the patterns deviate appreciably from the true patterns, but the deviations depend strongly upon the exact position of the horn in the field.*

Despite all the imperfections in the field, the resulting horn patterns measured in the collimated beam showed an improvement over measurements taken when the collimating lens was absent. (Compare figure 2.3 with figure 2.8.) Nevertheless, collimating systems less afflicted with

---

* It is possible to predict theoretically[4,6] the patterns that are measured in the non-uniform field of the lens. The calculations are extremely involved. Unfortunately there is as yet no method by means of which the knowledge of the horn pattern measured in the field of the lens could be utilized in deriving the true horn pattern.

diffraction effects are desirable. In the next two sections are described collimating systems intended to improve the characteristics of the collimated beam. These systems provide successively better approximations to a plane wave.

2.2 The Collimating Properties of System II.

Some preliminary measurements based on previous work[7] indicated that the large amplitude variation in the collimated beam of System I could be reduced greatly by tapering the incident illumination towards the edge of the lens. Physically this can be explained by the fact that by decreasing the field in the vicinity of the diffracting edge of the lens, the perturbations on the total field caused by the rim are smaller.

A convenient experimental arrangement by means of which tapering of the incident illumination can be achieved is shown in figure 2.9. This arrangement ensures that the incident wave front remains spherical so that collimation of the wave can take place in the usual way, that is, by transforming an incident spherical wave into an emergent plane wave.

In the diagram of figure 2.9, lens A is the collimating lens, whose emergent beam is the one of interest. Lens B, together with the source illuminating it, are only means of producing a spherical wave tapered in amplitude

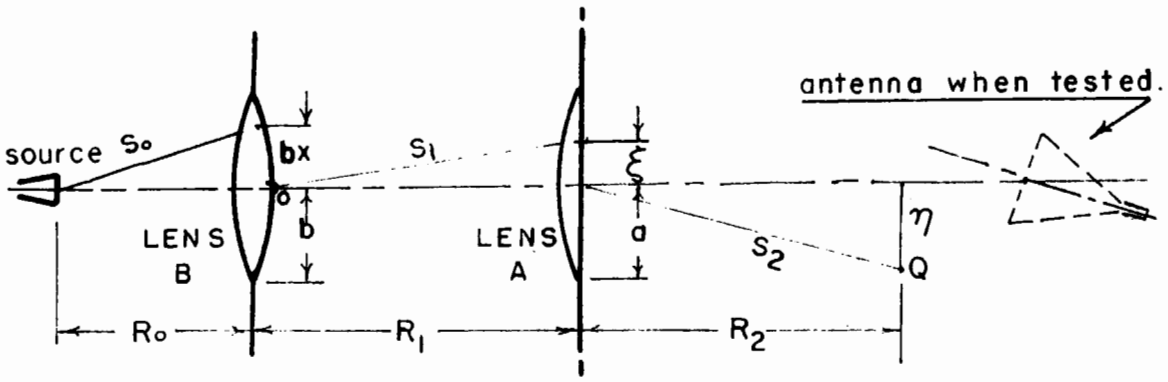

f_B = 50 cm.
$f_A = R_1 = 250$ cm.
R_o = 61.8 cm.
a = b = 25 cm.

SYSTEM II.

Fig. 2.9: System II, showing the experimental arrangement used to obtain tapered illumination over lens A.

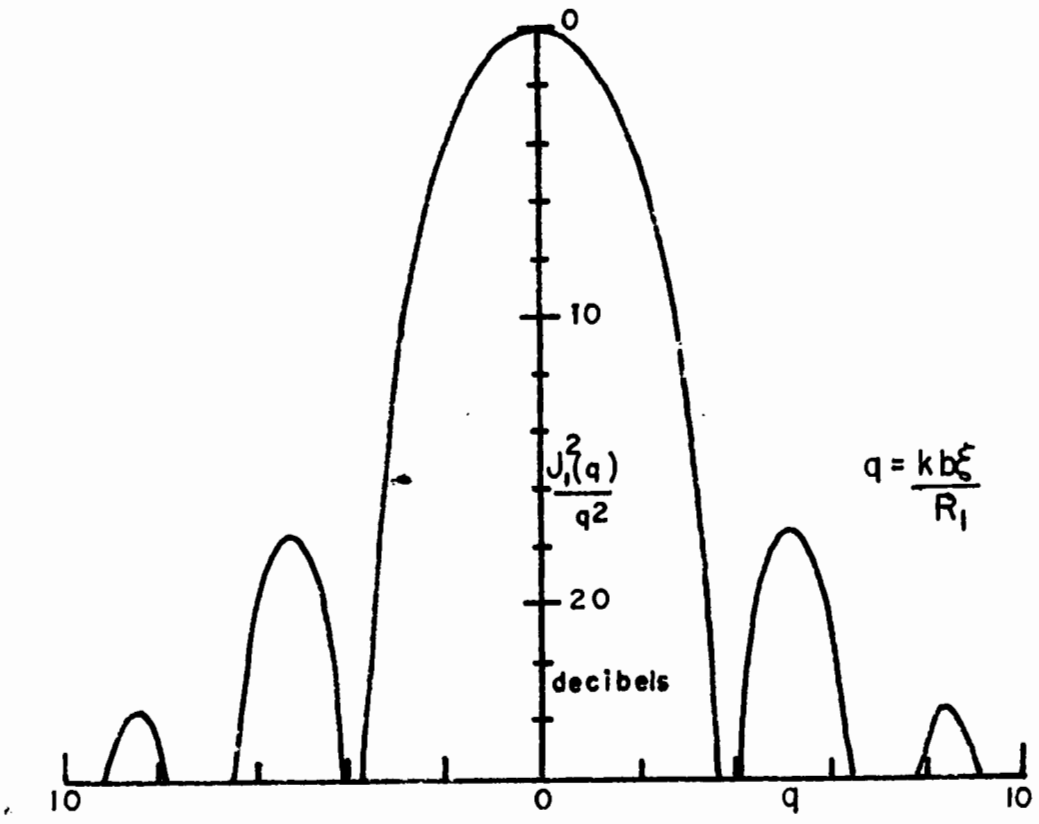

Fig. 2.10: The calculated intensity falling on lens A of System II, when lens B is illuminated uniformly.

over the collimator. The position of the source (i.e., its distance, R_o, from lens B) is adjusted so that the diffraction image of the first lens is focussed at the surface of the collimating lens (A). In view of the fact that in the diffraction image of lens B, energy is distributed over a region of lens A, and is more concentrated near the optical axis, tapering of the illumination is thus achieved. A theoretical analysis of this problem given below shows that the spherical phase front of the wave incident on lens A appears to be centered at point O (see figure 2.9). Hence in order to obtain a collimated, plane phase front emerging from lens A, the point O has to be coincident with the paraxial focus of the collimating lens.

In order to clarify the mode of action of this system, the mathematical analysis will be outlined. The field in the emergent beam of a lens is found with the aid of diffraction theory. It is shown in Appendix I that the amplitude at any point Q of the image space of a lens is given by the following expression:

$$(2.1)\quad u_Q = -\frac{jka^2 e^{-jkR}}{R} \int_o^1 u_i r \left(e^{\frac{-jka^2r^2}{2R}}\right) J_o\left(\frac{ka\xi r}{R}\right) dr$$

where u_Q is the amplitude of the field at a point Q in the image space.

u_i is the field in the aperture after passage through the lens, and will be assumed to be circularly symmetric about the optical axis in all subsequent discussion.

a is the radius of the lens.

r is the normalized distance of a point in the

aperture from the axis, such that (ar) measures the actual distance from the axis.

R is the distance from the center of the lens to the field point Q.

ξ is the perpendicular distance of the field point Q from the optical axis.

J_o is a Bessel function of the first kind and order zero.

and k again, is the wave number $(\frac{2\pi}{\lambda})$.

The above expression is quite general and is applicable to any lens when illuminated by an arbitrary wave whose amplitude and phase after passage through the lens are given by u_i. Hence to find the illumination over the collimating lens, the equation (2.1) has to be applied first in calculating the field in the image plane of lens B when this is illuminated uniformly by the source shown in the figure. Having calculated this field from lens B (which is the illumination falling on lens A) and taking account of the phase change produced by passage of the wave through lens A, the field u_i in the exit pupil of the collimating lens (A) can be found. This field u_i can then be substituted once again into the general expression (2.1) and the field calculated at any point of the collimated beam. The procedure outlined above will now be followed.

(1) The Diffraction Field of Lens B.

Consider lens B of figure 2.9, of radius b, illuminated by a spherical wave emanating from a source a distance R_o from the lens. The field u_{iB} , in the exit pupil

of this lens is given by:

$$(2.2)\quad u_{iB} = \frac{u_o}{R_o}\, e^{-jk\left(R_o + \frac{b^2x^2}{2R_o}\right) + \frac{jkx^2b^2}{2f_B}}$$

where u_o is a constant amplitude term. The term $\exp\left(\frac{jkx^2b^2}{2f_B}\right)$ is the phase shift introduced by lens B whose focal length is f_B. A substitution of u_{iB} into the integral of equation (2.1) gives:

$$(2.3)\quad u_{QB} = -\frac{jku_ob^2}{R_oR_1}\, e^{-jk(R_o + R)} \int_o^1 x\, e^{-\frac{jkx^2b^2}{2}\left(\frac{1}{R_o} + \frac{1}{R_1} - \frac{1}{f_B}\right)} J_o\left(\frac{kbx\xi}{R_1}\right) dx$$

where Q is some point an axial distance R_1 from the lens and a perpendicular distance ξ off the axis. It is seen from examination of the exponent in equation (2.3) that the condition:

$$(2.4)\quad \frac{1}{f_B} = \frac{1}{R_o} + \frac{1}{R_1}$$

ensures that the plane of observation (i.e., the field point Q) lies in the image plane of lens B, this image plane being a distance R_1 from the plane of the lens.

For the point Q in the image plane, such that equation (2.4) is satisfied, the integration in equation (2.3)

---

* The distance $S_o = (R_o^2 - b^2x^2)^{\frac{1}{2}}$ from the source to a point in the lens a radial distance bx from the axis (see figure 2.9) has been expanded to give the approximation for small x:

$$S_o \doteq R_o - \frac{x^2b^2}{2R_o}$$

that is used in the exponential of equation (2.2). S_o has been set equal to R_o in the amplitude term. Since only small displacements off the axis will be considered, a similar approximation will be made in the work to follow for the distances S_1 and S_2 in figure (2.9).

can be performed with the result that:

$$(2.5)\quad u_{QB} = -j\frac{k u_o b^2}{R_o R_1} e^{-jk(R_o+R)} \frac{J_1(q)}{q}$$

Where J_1 is a Bessel function of the first kind and first order, and $q = \frac{kb\xi}{R_1}$. This amplitude distribution u_{QB} is then used in illuminating lens A. It will be noted that the factor exp(-jkR) represents the phase of a spherical wave, while the variation in amplitude in the image plane is given by the factor $\frac{J_1(q)}{q}$, which provides the necessary amplitude tapering over the collimating lens A. The intensity of illumination is proportional to $\left[\frac{J_1(q)}{q}\right]^2$; a sketch of this intensity is shown in figure (2.10).

(2) <u>The Diffraction Field of the Collimating Lens A.</u>

If now the distance R_1 equals the focal length f_A of the collimating lens, (that is, if the center of lens B coincides with the position of the paraxial focus of lens A) then the spherical wave incident on lens A, in its passage through this lens, will be transformed into a wave with a plane phase front over the exit pupil of the lens, and with the aid of equation (2.5), u_i for lens A is found to be:

$$u_{iA} = u_o' e^{-jk(R_o+R_1)} J_1\left(\frac{kb\xi}{R_1}\right) \Big/ \left(\frac{kb\xi}{R_1}\right)$$

where u_o' is equal to the amplitude term $\left(-\frac{jkb^2 u_o}{R_o R_1}\right)$

Finally, a substitution of this value of u_{iA} into the general equation (2.1) gives the field at any point of the collimated beam emergent from lens A. The field is given by the expression:

$$u_{QA} = -j\frac{R_1}{R_2}\frac{a}{b}\,u_o' \left\{ e^{-jk\left(R_o + R_1 + R_2 + \frac{n^2}{2R_2}\right)} \right.$$

(2.6)

$$\left. \int_0^1 J_1\left(\frac{kbar}{R_1}\right) J_o\left(\frac{kanr}{R_2}\right) e^{-j\frac{ka^2r^2}{2R_2}}\, dr \right\}$$

where n is the perpendicular distance of the field point from the axis, and R_2 the axial distance of the field point from the lens A.

An exact evaluation of this integral is rather difficult. However, in view of the fact that the illumination of the lens is strongly tapered, and that much of the energy is concentrated over the central portion of the collimating lens, little energy is intercepted by the screen; hence the approximation that will be made in evaluating equation (2.6), namely that the lens is infinitely large (i.e., $a \to \infty$) will not cause serious errors in the final result for u_{QA}.

If a is allowed to go to infinity it is shown in Appendix II that the amplitude u_{QA} at some point Q of the collimated beam is given approximately by:

$$u_{QA} = \frac{u}{4\left(j\gamma' + \frac{\beta^2}{8}\right)} \left\{ 1 - 2\left(\frac{\beta}{\phi}\right)^4 \left[\left(\frac{kn}{2R_2\left(j\gamma' + \frac{\beta^2}{8}\right)}\right)^4 - \frac{2k^2n^2}{R_2^2\left(j\gamma' + \frac{\beta^2}{8}\right)^3} \right.\right.$$

(2.7)

$$\left.\left. + \frac{4}{\left(j\gamma' + \frac{\beta^2}{8}\right)^2} \right] \right\} \exp\left(-j\frac{kn^2}{2R_2} + j\frac{k^2n^2\gamma'}{R_2^2\left(4\gamma'^2 + \frac{\beta^2}{8}\right)} + \frac{\beta^2k^2n^2}{R_2^2\left(32\gamma'^2 + \frac{\beta^2}{2}\right)} \right)$$

Some constant phase and amplitude terms have been included in the factor u, and for simplicity the quantities β and γ' defined below are used: $\beta = \frac{kb}{R_1}$, $\gamma' = \frac{k}{2R_2}$. The symbol ϕ stands for the

first root of the Bessel function J_1 (i.e. $J_1(\phi) = 0$).

In the above expression for the field at a point Q in the image space of lens A, it is found that most of the phase variation (as function of η, the distance off the axis) arises from the quadratic term in η in the imaginary part of the exponential, while the major amplitude variation is given by the quadratic term in η in the real part of the exponential. (This information was of importance in suggesting the next collimating system studied in this chapter, which is discussed in section 2.3).

The amplitude and phase distribution, calculated from equation (2.7), in a plane parallel to the lens and at a distance R_2 = 200 cm. from it, are shown in figure (2.11). The calculated amplitude distribution indicates that tapering of the illumination incident on the collimator results in some improvement of this distribution over that obtained in the same plane using uniform illumination over the lens (that is as compared with System I). However, the phase distribution has shown some deterioration.

Further improvement of the amplitude distribution, accompanied by an improvement in the phase distribution is obtained by tapering the illumination over lens B by replacing the effective point source with a small horn antenna. Although no theoretical calculations for this modification have been made, extensive measurements were performed. These will be discussed below.

Referring once again to figure (2.9) which gives a schematic diagram of the experimental arrangement, the small

Page 30 comes after Page 28.

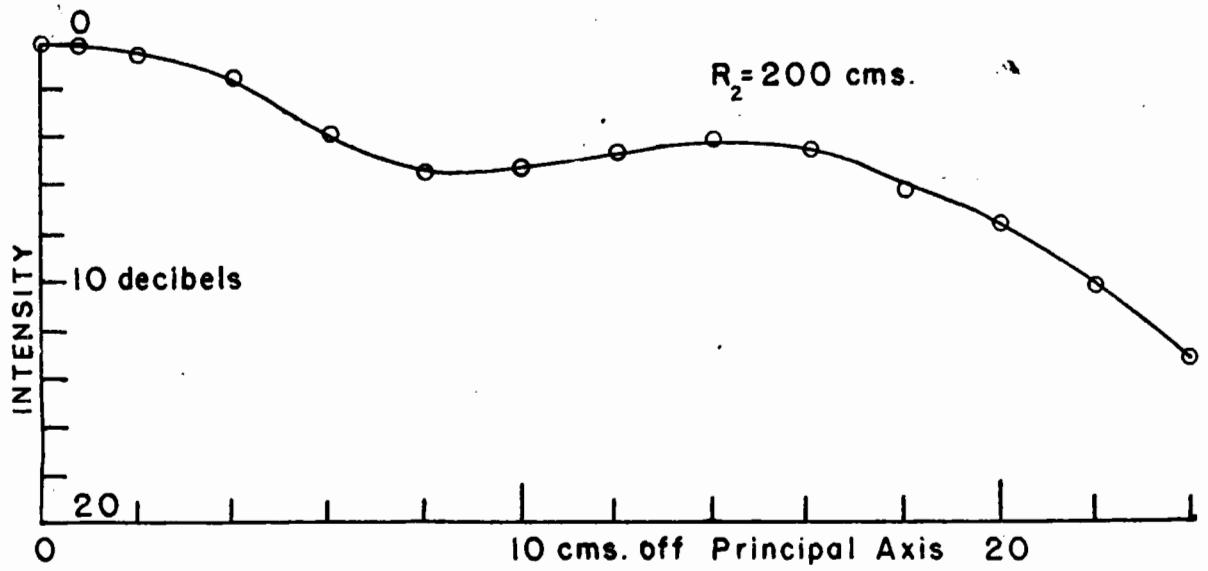

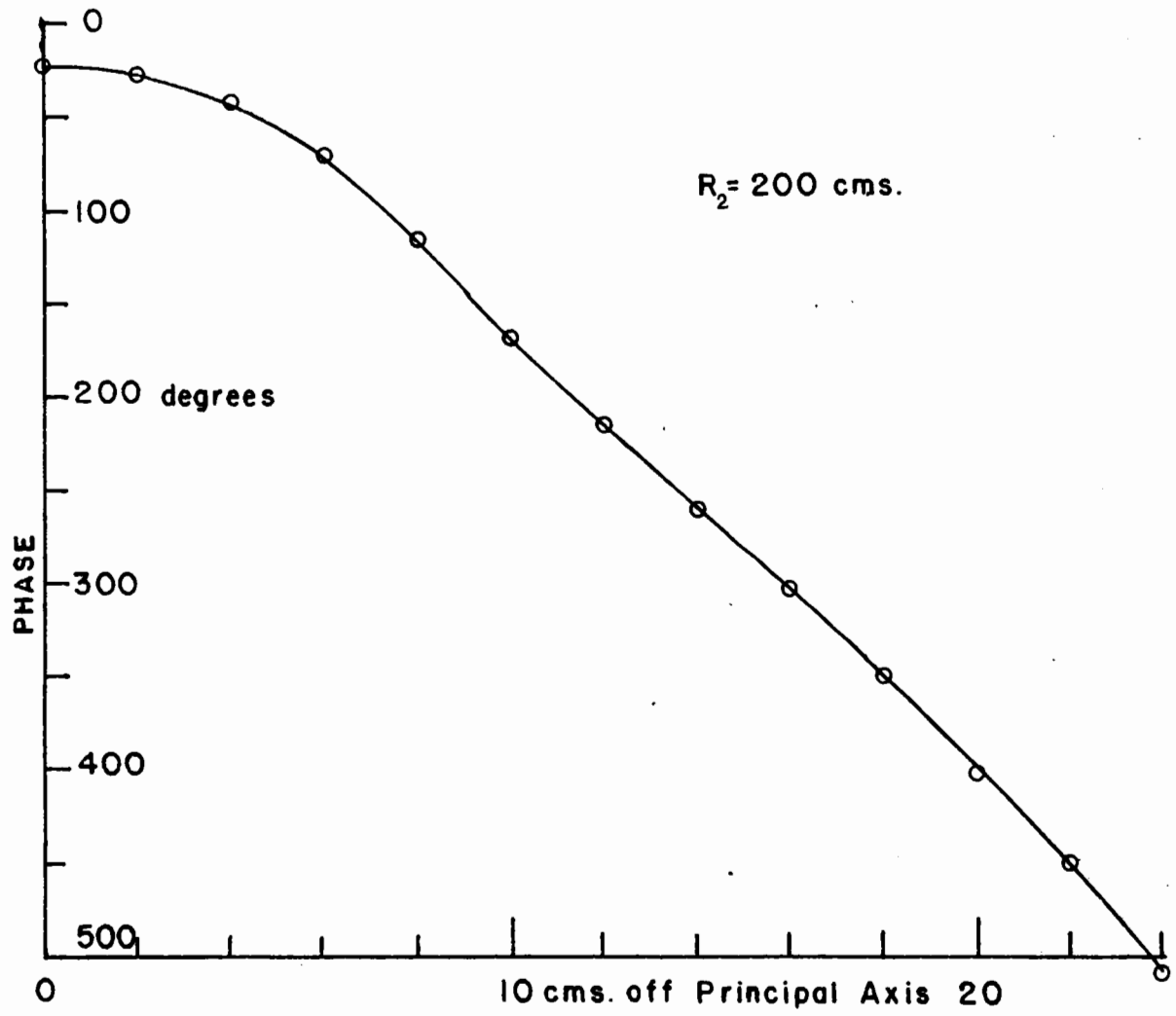

Fig. 2.11: Calculated intensity and phase in a plane 200 cms. from lens A of System II, for uniform illumination of lens B.

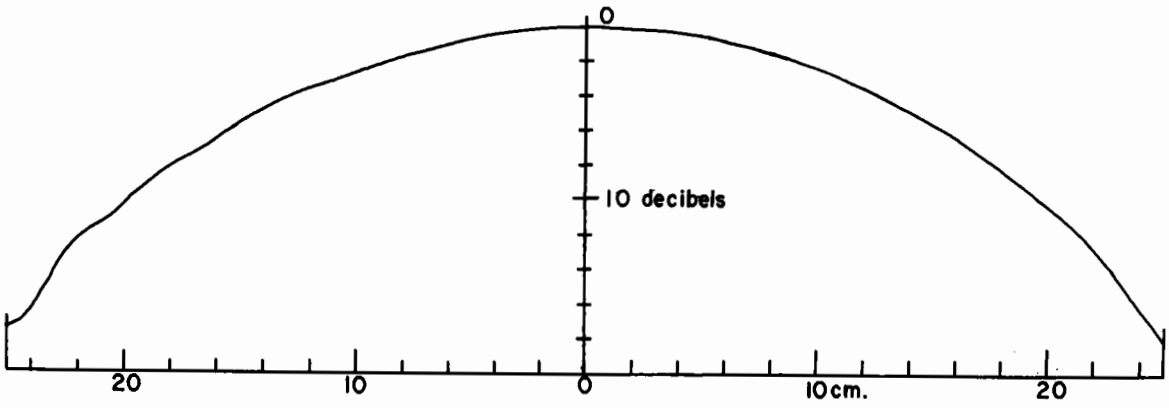

Fig. 2.12: Tapered intensity distribution over lens B of System II, provided by a small horn antenna.

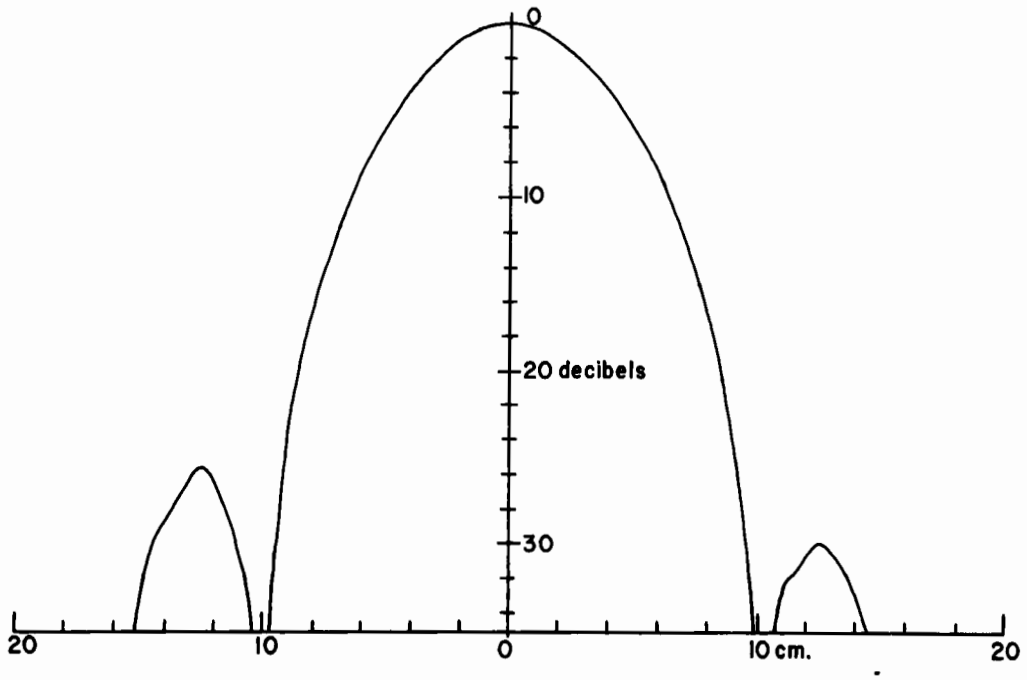

Fig. 2.13: Measured intensity distribution over lens A of System II.

horn used as the primary source produced a spherical wave over lens B that was slightly tapered towards the rim of the lens. (As mentioned in the previous paragraph such slight tapering aids in producing a good collimated beam from lens A.) The measured intensity distribution over lens B is shown in figure (2.12). The strongly tapered illumination measured over the collimating lens A is shown in figure 2.13. This illumination approaches the $\left(\frac{J_1(q)}{q}\right)^2$ distribution as calculated in equation (2.5). The major difference between the calculated and measured distribution over this lens is due to the slight tapering effected over lens B.

The measurement of the field distribution in the collimated beam was carried out in the same manner as for System I. Scans of the amplitude and phase distributions in various planes away from the lens are shown in figure (2.14a,&b). It will be noted that at a sufficiently large distance from the collimating lens (R_2 greater than about 150 cm.) the amplitude is quite uniform over an appreciable region of space and that there is in fact great improvement over the amplitude distribution obtained with System I (under uniform collimator illumination). However the phase shows no improvement over that obtained from System I; a somewhat greater overall departure from a plane phase front is noted. This greater phase variation is understandable because, due to tapering, only a small region of the lens is used effectively in collimation; if extremely sharp tapering were used the field would approach that of a point

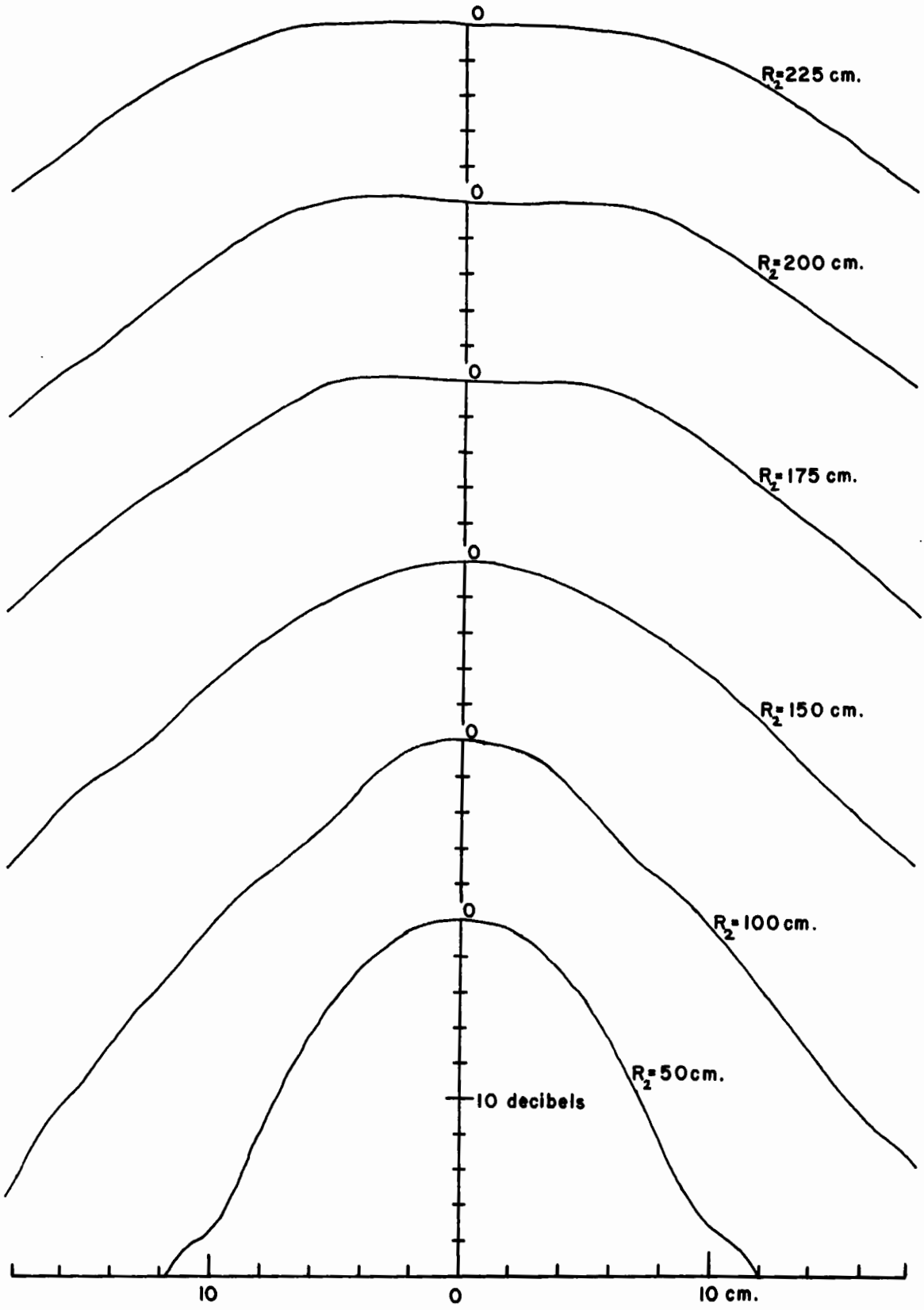

Fig. 2.14 (a): Intensity scans (H-plane) at distances (R_2) from lens A of System II.

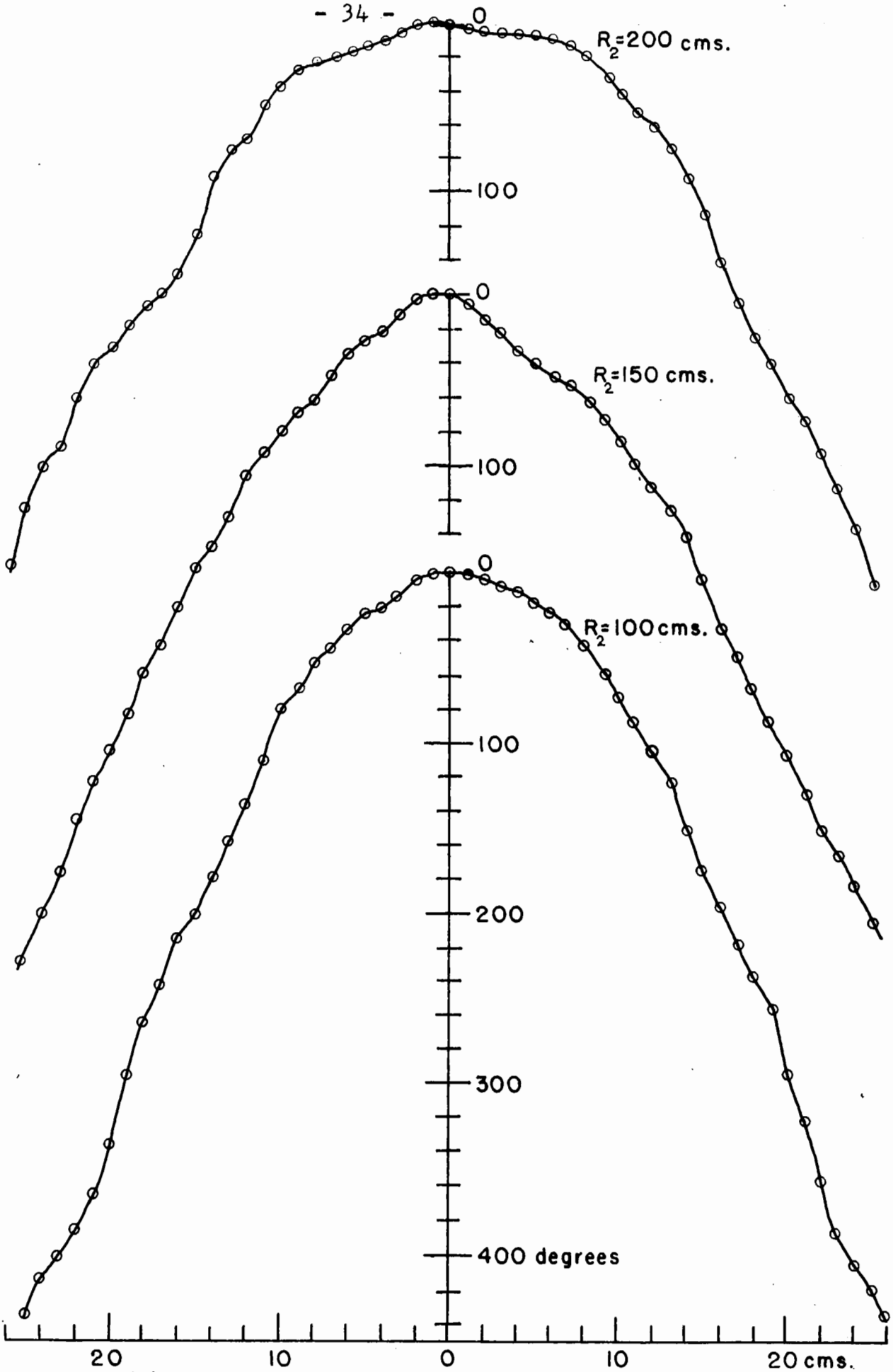

Fig. 2.14 (b): Phase scans (H-plane) at distances (R_2) from lens A of System II.

source and the benefit of collimation would be completely lost. This fact can be derived by an analysis of equation (2.7) but the subject will not be pursued further.

Horn Pattern Measurements in the Collimated Beam of System II.

Having examined above the properties of the collimated beam of this system, the radiation patterns of the three microwave horns, measured in a manner identical to that described previously, will now be discussed. Some of the patterns, measured in the E and H-planes of polarization are shown in figure (2.15). The results are seen to be satisfactory for the horns of smaller aperture size. The measured 10λ horn patterns agree very well with the true patterns of that horn, and great improvement can be seen when comparison is made with the patterns obtained with System I. (cf. figure (2.8) with figure (2.15)) The reproducibility of the patterns measured using System II is also superior because of the less rapid variation of the field as a function of distance from the lens. The results are less satisfactory for the 26λ horn because the phase undergoes too large variations over the mouth of this horn.

Although the system discussed in this section provided a very satisfactory collimated beam as far as amplitude is concerned, the phase variations, however, are such that the patterns of antennas with apertures larger than about 10λ cannot be measured with any degree of accuracy. For that reason a somewhat different method of

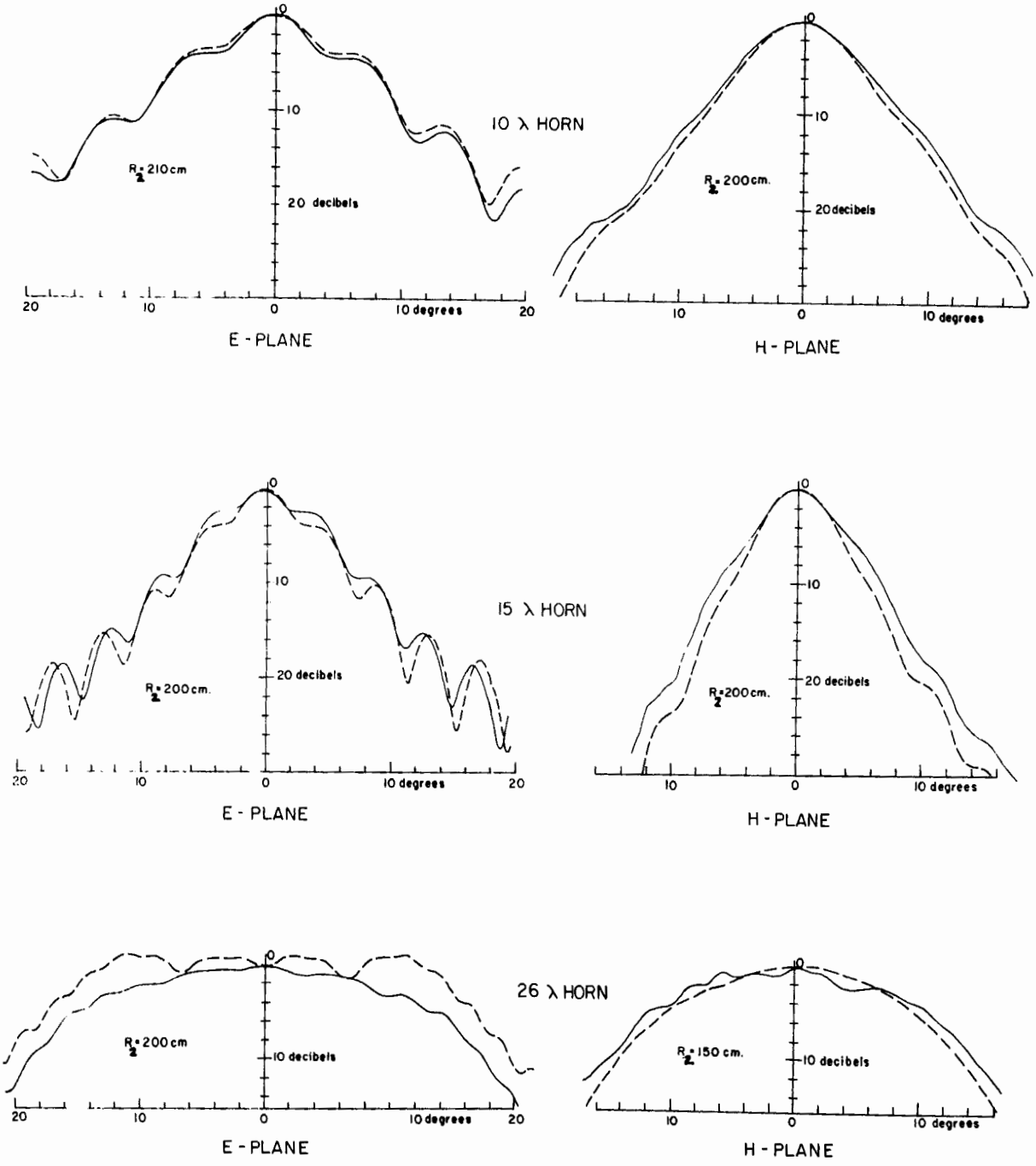

Fig. 2.15: Horn patterns measured at distances (R_2) from the lens A of System II. The true patterns are shown in a dashed line.

collimation is discussed in the next section, whose aim is to improve the phase characteristics of the collimated beam, and retain the good amplitude distribution obtained with the system described here.

2.3 The Collimating Properties of System III.

In the foregoing section it was seen that by tapering the illumination over a collimating lens, the amplitude variations in the collimated beam were greatly reduced. The phase distribution however, still deviated strongly from thatof a plane wave. This section describes a method of improving the phase in the collimated beam by accompanying the tapering in illumination with a proper adjustment of the phase over the exit pupil of the collimating lens.

In the approximate expression derived for the field in the image space of System II (equation (2.7)) it was pointed out that the phase variations in a plane parallel to the lens were largely quadratic. (This was in fact confirmed by the measurements as well as the calculations). An examination of equation (2.7) showed that by suitably adjusting the dimensions R_o and R_1 of figure (2.9), so as to change the phase distribution of the wave illuminating the collimating lens, much of this quadratic variation could be eliminated in a particular region of the image space. However, rather than re-examine System II, a direct theoretical analysis will be made of a more ideal collimating system that has a Gaussian amplitude distribution and a

quadratic phase variation over the exit pupil of the collimating lens.

An illumination over the exit pupil of the following form is assumed:

$$(2.8)\quad u_i = e^{-\xi^2(\mu + j\gamma)}$$

where ξ is again the radial distance from the optical axis and μ and γ are real constants. The first term in the exponent represents the above mentioned Gaussian amplitude distribution, and the second term the quadratic phase variation.

Substituting this value for u_i into the general expression (2.1) yields the following result for the amplitude u_Q at any point of the image space of the lens, again under the assumption that the tapering is sufficient to allow integration over an infinite domain ($a \to \infty$) rather than over the finite lens.

$$(2.9)\quad u_Q = -jk\, e^{-jk\left(R_2 + \frac{\eta^2}{2R_2} - \frac{\eta^2 k^2 \gamma_o}{4R_2^2(\mu^2+\gamma_o^2)}\right) - \frac{k^2\eta^2\mu}{4R_2^2(\mu^2+\gamma_o^2)}}$$

where $\gamma_o = \gamma + \frac{k}{2R_2}$, η is again the perpendicular distance of the field point Q from the axis, and R_2 is the axial distance of Q from the lens. It will be noted that along the axis of symmetry ($\eta = o$) the phase varies linearly with distance R_2 from the lens as would be the case in a plane wave. However, some distance η off the axis a quadratic phase error exists for general values of R_2, μ and γ_o. But because of the difference in sign of the two coefficients

of η^2 in the imaginary part of the exponent, it is possible with a suitable choice of μ and γ_o, to eliminate this phase variation over a plane at a specified distance R_2 from the lens.

With this plane chosen a given distance R_2' from the lens, and for a given amount of taper over the lens (governed by the value of μ), the amount of quadratic phase variation necessary in the exit pupil of the lens is given by

$$(2.10)\quad \gamma = \gamma_o - \frac{k}{2R_2'} = -\frac{k}{4R_2'}\left(1 \pm \sqrt{1-\left(\frac{4\mu R_2'}{k}\right)^2}\right)$$

(The negative result implies that a converging, rather than a diverging, wave is required in the exit pupil.) With this value of γ, the amplitude distribution, u_Q, in the plane at R_2' now becomes:

$$(2.11)\quad u_Q = -\frac{jke^{-jkR_2'}}{2R_2'(j\gamma_o + \mu)}\, e^{-2\mu\eta^2 / 1 \pm \sqrt{1-\left(\frac{4\mu R_2'}{k}\right)^2}}$$

Hence it is seen that by a proper choice of amplitude and phase over the lens, there exists a plane at some distance R_2' over which the phase remains constant and the amplitude varies slowly. Further consideration shows that even outside this plane, the phase varies quite slowly. This variation (together with the behaviour of the amplitude) is sketched in figure (2.16) for a given choice of γ and μ.

Choice of Parameters

The above theoretical considerations are approximate in that an integration over an infinitely large lens was

assumed to be valid.** This assumption becomes better and better the more the energy is tapered towards the rim of the lens, but too much taper over the lens causes more amplitude variation in the plane at R_2' than can be tolerated for antenna measurements. In order that any experimental arrangement should perform according to the theoretical predictions while still giving a slowly varying amplitude in the plane at R_2', a criterion as to the intensity that can be tolerated at the rim was established. It was found experimentally (with the arrangement of System III, to be described later) that with the intensity at rim ($\xi = a$) about $\frac{1}{1000}$ of that at the lens center, a phase variation in good agreement with theory could be obtained. With less taper than this, the phase distribution in the plane a distance R_2' from the lens deteriorated. From equation (2.8) one then obtains the result that

$$e^{-2\mu a^2} \leq .001 \quad \text{or} \quad \mu \geq \frac{3.46}{a^2}$$

Another criterion for μ results from equation (2.10). Since is a real quantity, it is necessary that

$$\mu \leq \frac{k}{4R_2'}$$

Hence μ must lie between the limits

$$(2.12) \quad \frac{3.46}{a^2} \leq \mu \leq \frac{k}{4R_2'}$$

For the size of lens that was available ($a = 25$ cm.) and at the working wavelength of 1.235 cm., the above criteria are satisfied for $R_2' = 145$ cm. and $\mu = .00875$. In parti-

** An exact method of evaluating the integral for a finite lens is outlined in Appendix III.

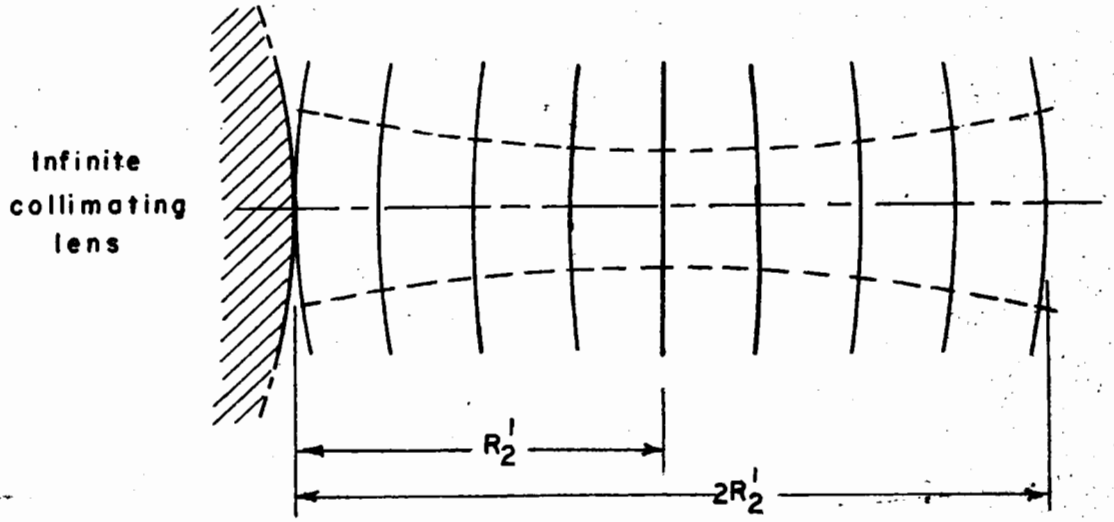

Fig. 2.16: The phase and intensity variation in the emergent beam of an ideal collimating system, for the choice of parameters: $-\gamma = \mu = \frac{k}{4R_2'}$ ..Dashed lines show the locus of points where the intensity is 3db. below that on the axis.

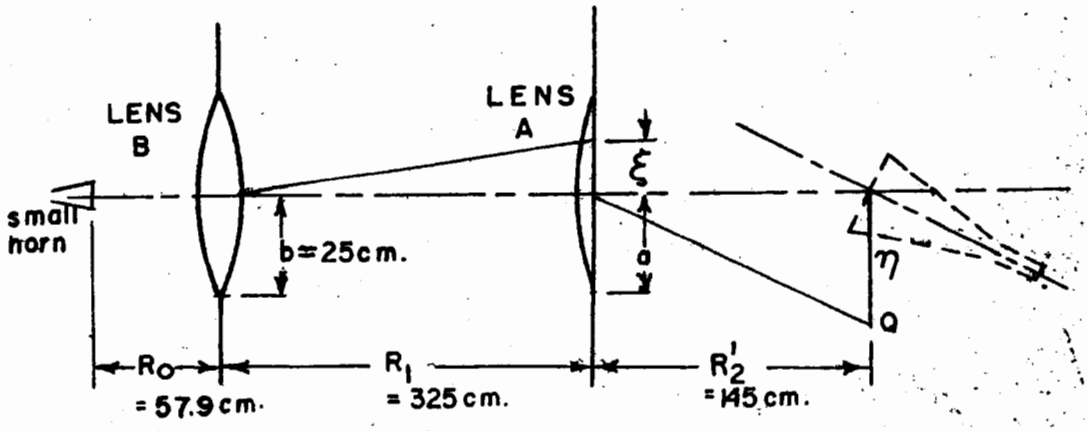

Fig. 2.17: System III, showing the experimental arrangement used to obtain a quadratic phase variation and an approximate Gaussian amplitude distribution over lens A.

cular, these values satisfy the condition $\mu = \frac{k}{4R_2'}$; with this condition the phase varies almost symmetrically on either side of the plane, a distance R_2' from the lens, over which the phase is constant.

Having demonstrated, theoretically, a means of improving the phase distribution in a collimated beam emerging from a lens, an experimental arrangement for attaining the field in the exit pupil of the lens necessary to achieve this result will now be discussed.

In figure (2.17) is shown the apparatus used to obtain the quadratic phase variation and an approximation of the Gaussian amplitude distribution over the collimating lens of what will be called System III. The arrangement providing this illumination differs only in detail from that used in illuminating the collimating lens of System II.

In System III, the diffraction image of lens B is again arranged to coincide with lens A. It will be recalled from the previous section (equation (2.5)) that the amplitude distribution in the diffraction image of a uniformly illuminated lens is of the form $\frac{J_1(\beta\xi)}{\beta\xi}$ where ξ is the radial distance from the axis. For small values of ξ, comparison of the series expansions of a Gaussian function and the above Bessel function shows that

$$\frac{J_1(\beta\xi)}{\beta\xi} \sim \frac{e^{-(\beta^2\xi^2)/8}}{2}$$

Hence, the Bessel function amplitude distribution would provide

a rough approximation of the desired Gaussian distribution over part of the lens. However, it was found that a better approximation of a Gaussian amplitude distribution can be obtained by tapering the illumination falling on lens B. A small horn was once more used for this purpose.

It was mentioned above that for a choice of the taper factor (μ) the equality

(2.13) $\mu = \frac{k}{4R_2'}$ gave good results.

Substituting this value into equation (2.10) gives the value of the phase factor (γ) required, namely: $\gamma = -\frac{k}{4R_2'}$. The quadratic phase distribution required in the exit pupil of the lens is then $e^{+jk\xi^2/4R_2'}$ and this distribution can be obtained by adjusting the distance R_1 (figure (2.17)) as will be shown.

In Section 2.2 it was found that the phase front of the field at the image plane of a lens is spherical and centered at the center of the lens. As in System II, such a spherical wave illuminates lens A of figure (2.17) provided:

$\frac{1}{f_B} = \frac{1}{R_o} - \frac{1}{R_1}$ where lens A is situated at ($R = R_1$), the image plane of lens B. Again, by taking account of the phase shift introduced by lens A, the field emerging from this lens can be written:

$$u_{1A} = u_o(e^{-\mu \xi^2})\, e^{\frac{-jk\xi^2}{2}\left(\frac{1}{R_1} - \frac{1}{f_A}\right)}$$

where u_o is a constant of proportionality, $e^{-\mu \xi^2}$ is the Gaussian amplitude distribution obtained approximately with the arrangement shown, and

$$e^{-j\frac{k\xi^2}{2}\left(\frac{k}{2R_1} - \frac{k}{2f_A}\right)} = e^{+ j\frac{k\xi^2}{4R_2'}}$$

is the quadratic phase term desired.

The conditions necessary to determine R_o and R_1 are then:

$$\gamma = -\frac{k}{4R_2'} = \frac{k}{2R_1} - \frac{k}{2f_A}$$

and $$\frac{1}{f_B} = \frac{1}{R_o} + \frac{1}{R_1}$$

Using these relationships, the dimensions shown in figure (2.17) were determined. The intensity distribution over the lens, and the characteristics of the collimated field achieved with this arrangement are discussed below.

Field measurements were made at the exit pupil of lens A and in regions beyond this lens in the same manner as with previous systems. The intensity of illumination over lens A is shown in figure (2.18a) together with the intensity distribution in the collimated beam for the planes of measurement, neighbouring the plane at (R_2' = 145 cm.). The corresponding phase distributions are indicated in figure (2.18b). From these measurements, a remarkable improvement in the phase distribution of the collimated wave over that found in System II, can be seen. The intensity varies

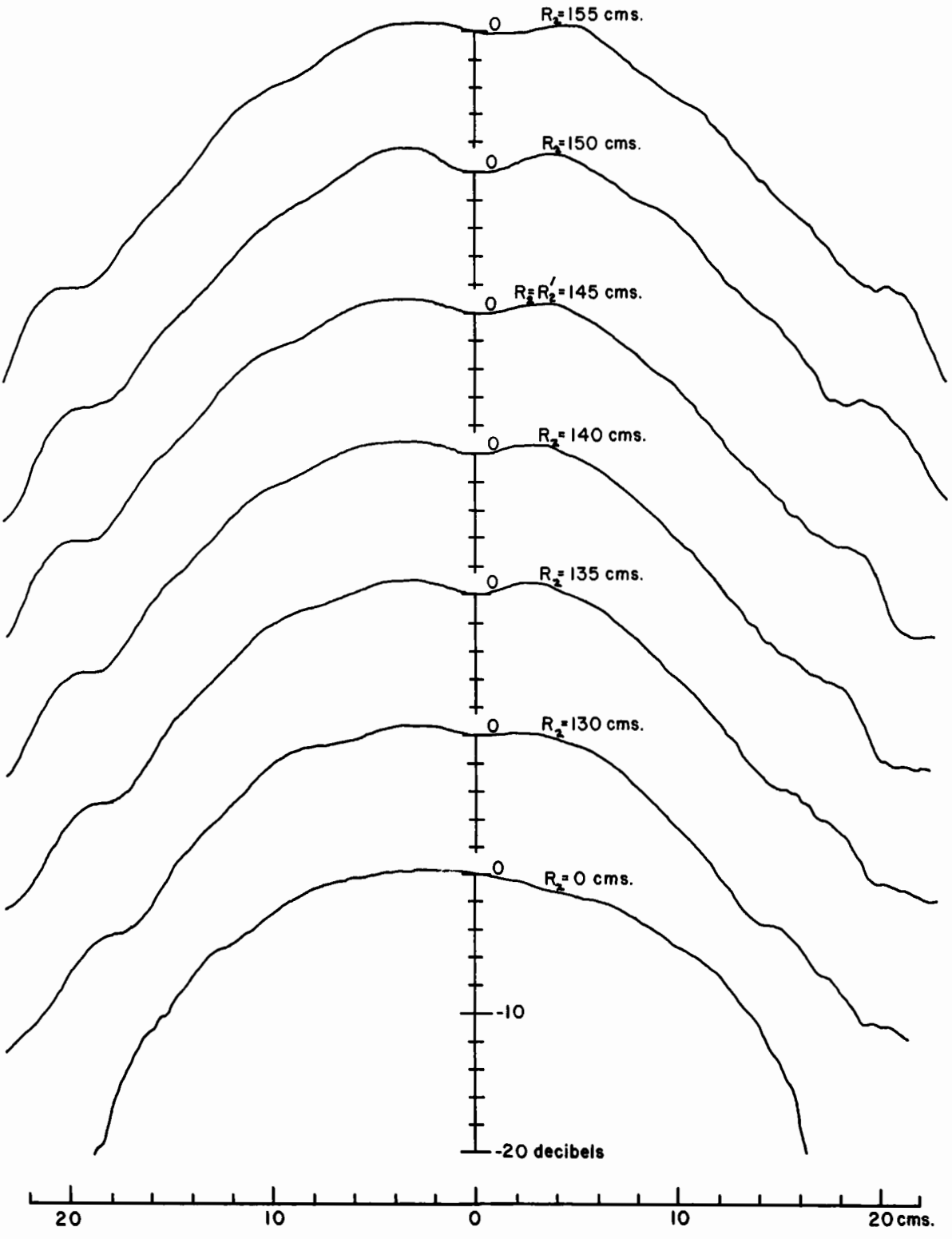

Fig. 2.18a: Intensity scans (H-plane) at various distances (R_2) from lens A of System III.

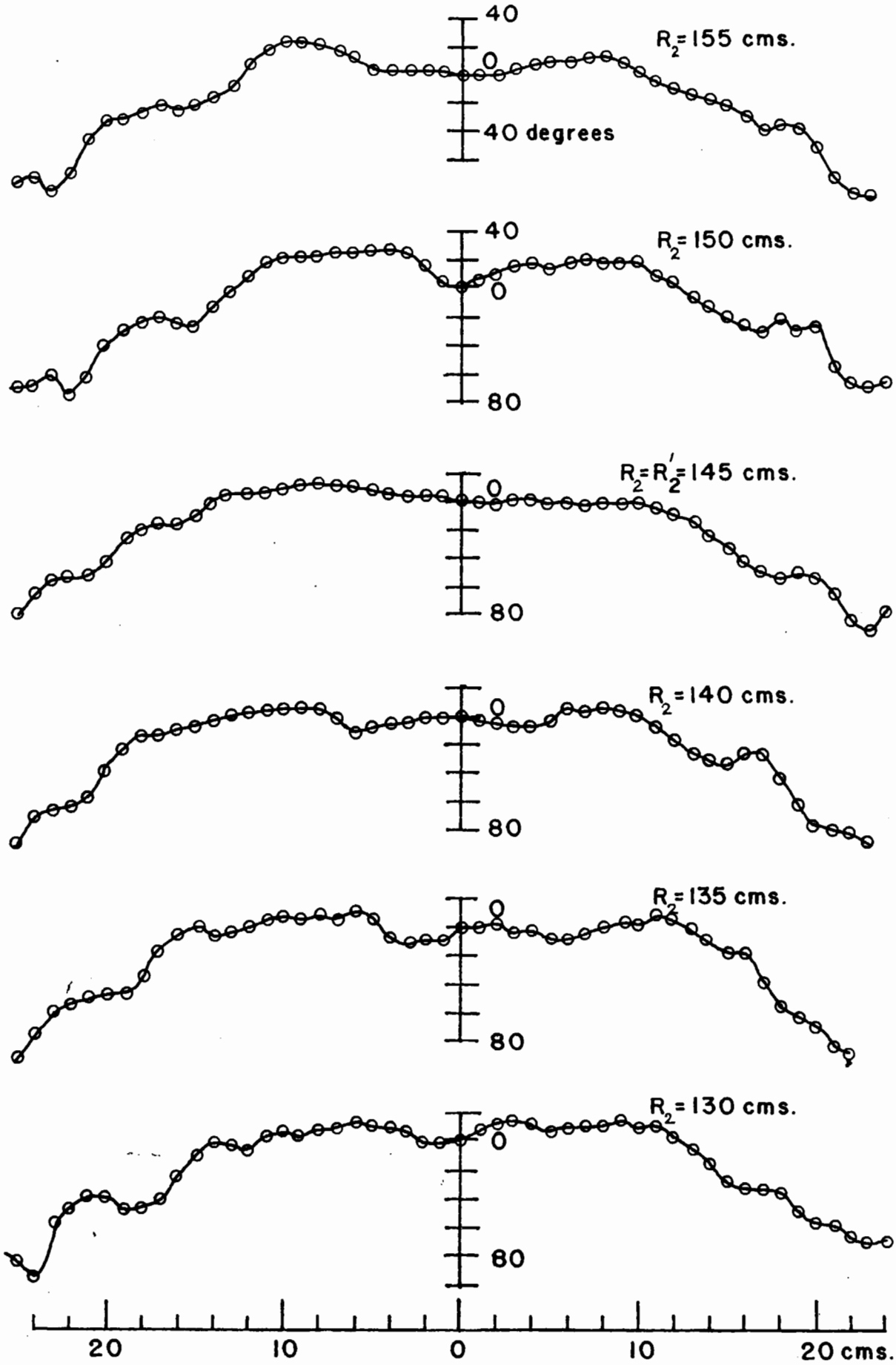

Fig. 2.18b: Phase scans (H-plane) at various distances (R_2) from lens A of System III.

slowly in this region of good phase, but is uniform over a smaller volume of space than was the intensity distribution in System II.

Thus, although the region of nearly constant intensity achieved with System III is not as large as that attained in System II, both the intensity, as well as the phase are almost uniform over a considerable volume of the collimated beam of System III. This volume is centered at $R_2 = R_2'$ and the results are in good agreement with the approximate theory derived. Horn radiation patterns measured in the vicinity of $R_2 = R_2'$ in the collimated beam of System III are now discussed.

Horn Pattern Measurements in the Collimated Beam of System III

The radiation patterns of the three electromagnetic horns were measured in the same manner as described before; the results of these measurements are presented in figure (2.19). Good agreement between the true patterns and those measured using System III can be seen for the H-plane patterns of the 10 λ and 15 λ horns.

To show that adjustments in the position of the antenna in the field are not too critical, these H-plane patterns were taken at the various distances (R_2), away from the lens, shown on the graphs. The E-plane pattern measurements were not so successful however. Errors in the E-plane pattern of the 10 λ horn are greater than they were using System II. This fact is explained by the sharper fall-off in

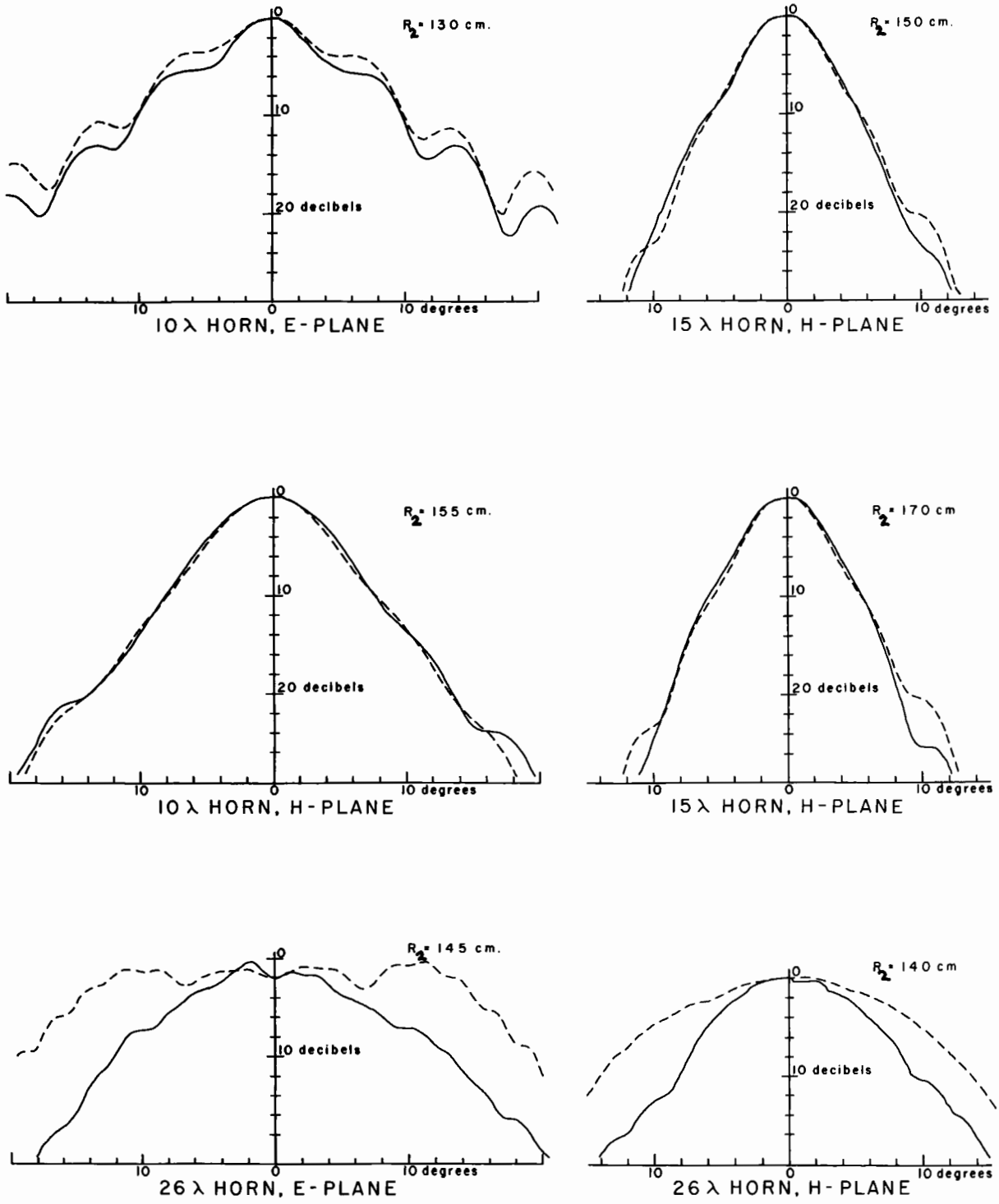

Fig. 2.19: Horn patterns measured at distances (R_2) from lens A of System III. The true patterns are shown in a dashed line.

intensity with distance away from the axis found in the collimated beam of System III; the H-plane patterns for these smaller horns were not significantly effected by this variation of the field, because an inherent taper in intensity, which is due to the electromagnetic field configuration in a rectangular horn, already exists in the H-plane over the mouth of the horn.(1) (This inherent taper does not exist in the E-plane over the mouth of a horn.) But the variations in amplitude of the collimated field of System III were too drastic to allow good results with the 26 λ horn even in the H-plane pattern measurements.

A means of extending the region of uniform amplitude in the collimated beam of System III is suggested in the brief summary of the three systems so far discussed, that follows.

2.4 A Summary of the Properties of Systems I, II and III.

The results of measurements in the collimated field of System I (a lens mounted in a screen and illuminated uniformly by a small source) showed severe amplitude and phase variations caused by diffraction at the edge of the lens. Horn radiation patterns measured in various regions of the collimated beam were both inaccurate and inconsistent because of this field variation. However, the magnitudes of the amplitude and phase fluctuations were smallest at the surface of the collimating lens (figures (2.6) and (2.7)) and this information suggested

another system for measuring the patterns of antennas and scattering objects that will be described in the next chapter.

In System II, much improvement in the amplitude distribution in the near field of the collimating lens resulted from tapering the illumination falling on that lens, but the phase variation in the collimated beam was too great to allow accurate measurements of antenna radiation patterns for antennas having apertures more than about 10λ in size.

In System III, tapering of a slightly different form, combined with adjustment of the phase over the collimating lens, led to great improvement in phase in one region of the near field, compared with the corresponding phase distribution in the near field of System II. The region of good amplitude, however, was smaller than that obtained using System II, and this fact imposes the major restriction in the use of System III for measurements of the characteristics of large antennas. But by increasing the diameter of the collimating lens, it will now be shown that this restriction can be overcome.

With the equality (2.12) ($\mu = \frac{k}{4R_2'}$) satisfied, the amplitude distribution in the collimated beam at $R_2 = R_2'$ is (from equation (2.11))

$$(2.14) \quad u_Q = -jke\frac{-jkR_2'}{2R_2'(j\gamma+\mu)} e^{-2\mu\eta^2}$$

where μ describes the taper in intensity over the collimating lens (i.e., $|u_i|^2 = e^{-2\mu\xi^2}$), and μ must satisfy the criterion

(found to be necessary for good agreement between the predicted field and the measured field):

(2.12) $\mu \leq \frac{3.46}{a^2}$ where a is the radius of the collimating lens. Hence to decrease the amplitude variation in the collimated beam, μ must be decreased (by equation (2.14)) and this can only be done, in view of the criterion (2.12), if the lens radius (a) is increased.

Following a description in the next chapter of the final collimating system tried, and an outline of the experimental methods in Chapter IV, a quantitative comparison of all systems will be made in the Conclusion.

Chapter 3.

A MICROWAVE COLLIMATING SYSTEM FOR SPECIAL ANTENNA AND SCATTERING MEASUREMENTS.

A means of taking advantage of the relatively small fluctuations in amplitude and phase found in the emerging wave very close to the collimating lens of System I is described in this Chapter. The region very close to the lens surface in System I could not be used for antenna measurements with that system because of the space required for free rotation of the antenna. This difficulty is eliminated by mounting an antenna (or scatterer) at the surface of the collimating lens and rotating both the lens and antenna as a unit. This arrangement, called System IV, is sketched in figure (3.1). The system is particularly applicable to the special problem of studying the radiation characteristics of antennas having a well defined plane aperture, or the scattering properties of plane scatterers. But if the antenna or scatterer consisted of a system of elements spread over a sizable volume, such that a number of elements were in regions of more severe field variations than found at the surface of the lens, the advantages of System IV would be lost.

The properties of System IV were evaluated, in the same manner as were those of previous systems, by measuring the radiation patterns of the three electromagnetic horns in the field collimated by the lens. In addition, measurement of the back-scattering pattern of a large disc was undertaken.

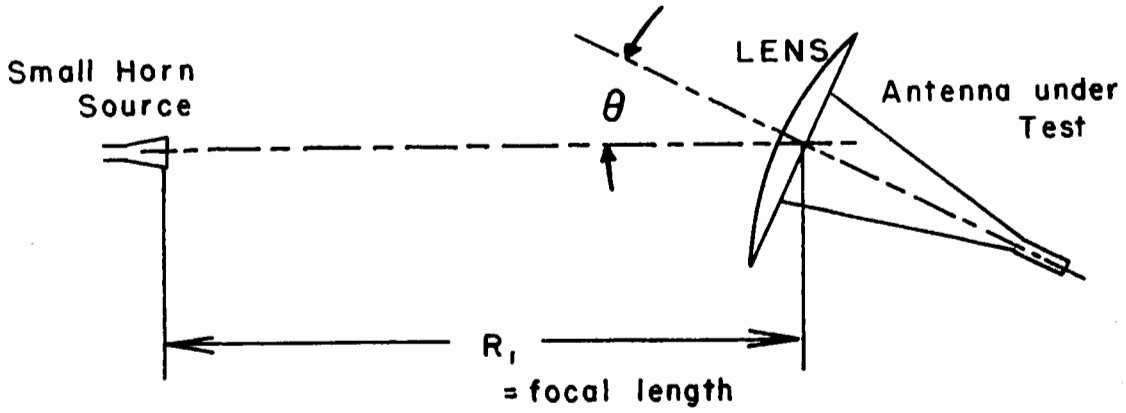

Fig. 3.1: System IV as used for antenna measurements. The lens and antenna are rotated together through angles (θ).

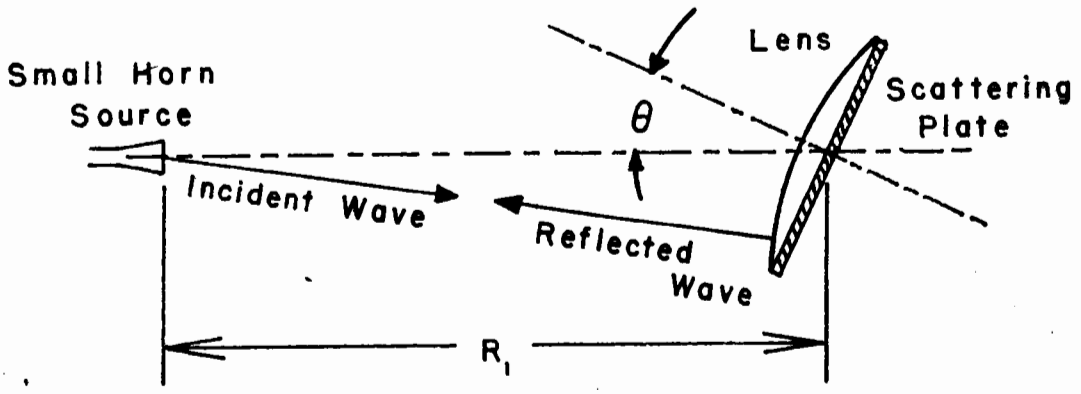

Fig. 3.2: System IV as used for back-scattering measurements.

using System IV. The results of these measurements will be presented before any mention is made of possible causes of the inaccuracy found in the measurements.

3.1 The Measurement of Horn Radiation Patterns Using System IV.

A selection of horn patterns measured using System IV is given in figure (3.3). Two lenses, lens A and lens C (described in Table II) were tried as the collimating lens. Both lenses gave good results, but lens A was slightly more satisfactory than lens C (for example, compare pattern (3) with pattern (4) in figure (3.3)). The improvement in accuracy of the measured horn patterns is apparent when comparison is made with the results using System I (figure (2.8)).

The increased accuracy in the patterns is attributed to the relatively small variations in amplitude and phase of the field near the collimating lens, where the horns were mounted. The reliability of the measured patterns is also greater using System IV as compared with System I. This is because the position of the horns was well defined in System IV: the horns were mounted with their aperture rims in contact with the surface of the lens, and they could be easily centered on the principal axis of the lens. The patterns were also relatively insensitive to the distance of the source from the lens. The source could be moved several centimeters with very little change in the measured horn pattern.

System IV then, is a simple improvement of System I

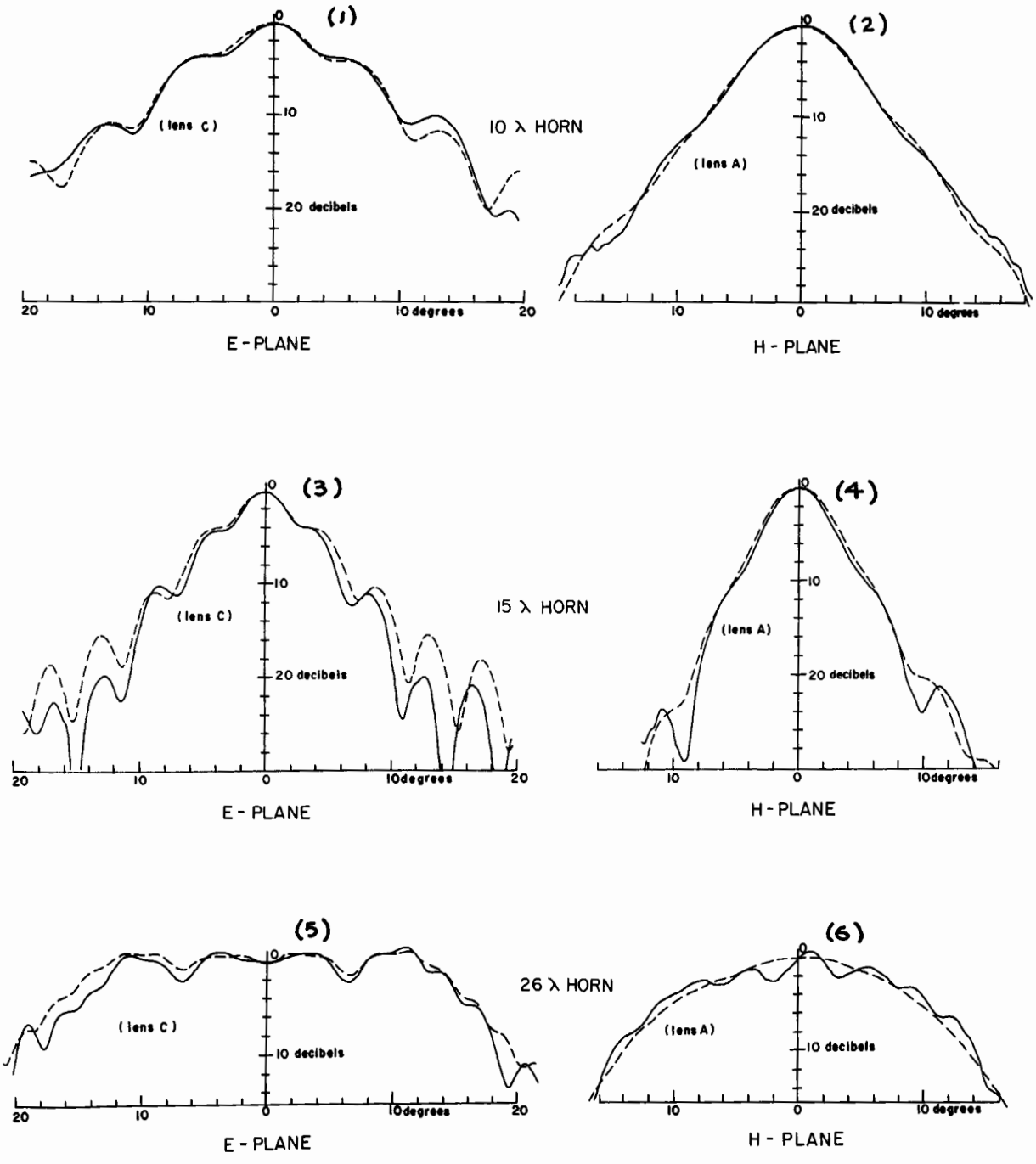

Fig. 3.3: Horn patterns measured using System IV, for the two lenses (A and C) indicated. The true patterns are shown in a dashed line.

useful in the measurement of the radiation characteristics of antennas having a plane aperture. The other application of System IV mentioned, the measurement of back-scattering patterns of plane scatterers, is described below.

3.2 The Measurement of the Back-Scattering Pattern of a Circular Plate, Using System IV.

Ideally, the collimating action of a lens effectively removes a small source at the focus to infinity (as in both Systems I and IV). With the source at infinity, (i.e., with a plane wave) a measurement of the relative amount of energy scattered backwards towards the source by a scattering object, as a function of the orientation of the object, furnishes what is called the back-scattering pattern of the scatterer. It can be easily shown that the ideal back-scattering pattern of a large disc rotated about a diameter perpendicular to the direction of propogation of the plane wave, is given approximately by:*

$$I = \left(u_0 \frac{J_1(q)}{q}\right)^2 \cos^2\theta,$$ where u_0 is a constant of proportionality, and $q = kD\sin\theta$, with D the diameter of the plate, θ the angle of rotation relative to the direction of propogation, and k the wave number ($\frac{2\pi}{\lambda}$).

The particular arrangement of System IV, used to measure the back-scattering pattern of a circular aluminum

---

* This result is subject to the assumptions of the scalar diffraction theory of Kirchhoff. More rigorous but similar solutions, taking polarization into account are available.(8)

plate is shown in figure (3.2). A small horn illuminated lens A (Table II) with a spherical wave of nearly constant amplitude. This horn was also used as the receiving antenna. (Details of the transmitting and receiving apparatus are given in Chapter 4.) The plate was 50 cm. in diameter and was mounted in contact with the plane surface of the lens. The plate and lens were rotated in the direction of the magnetic field.

Back-scattering patterns of the plate, measured for two distances (R_1) separating the lens from the source, are shown in figure (3.4). The theoretical pattern: $\cos^2\theta \left(\frac{u_o J_1(q)}{q^2}\right)^2$, is plotted in a dotted line for comparison. The agreement between the measured patterns and the ideal pattern is relatively good; the inaccuracies in the back-scattering measurements that do exist help to illustrate what sources of error are important in System IV. These errors will be discussed explicitly in the following section.

3.3 Sources of Error in the Measurement of Antenna and Scattering Patterns, Using System IV.

In the antenna and scattering patterns measured using System IV, it is believed that sources of error depending on experimental technique, such as those due to misalignment or room reflection, were small. Other sources of error are listed and discussed below.

(a) Lens Aberrations: Referring to Table II, it is seen that both lenses tried with System IV (lenses A and C) were

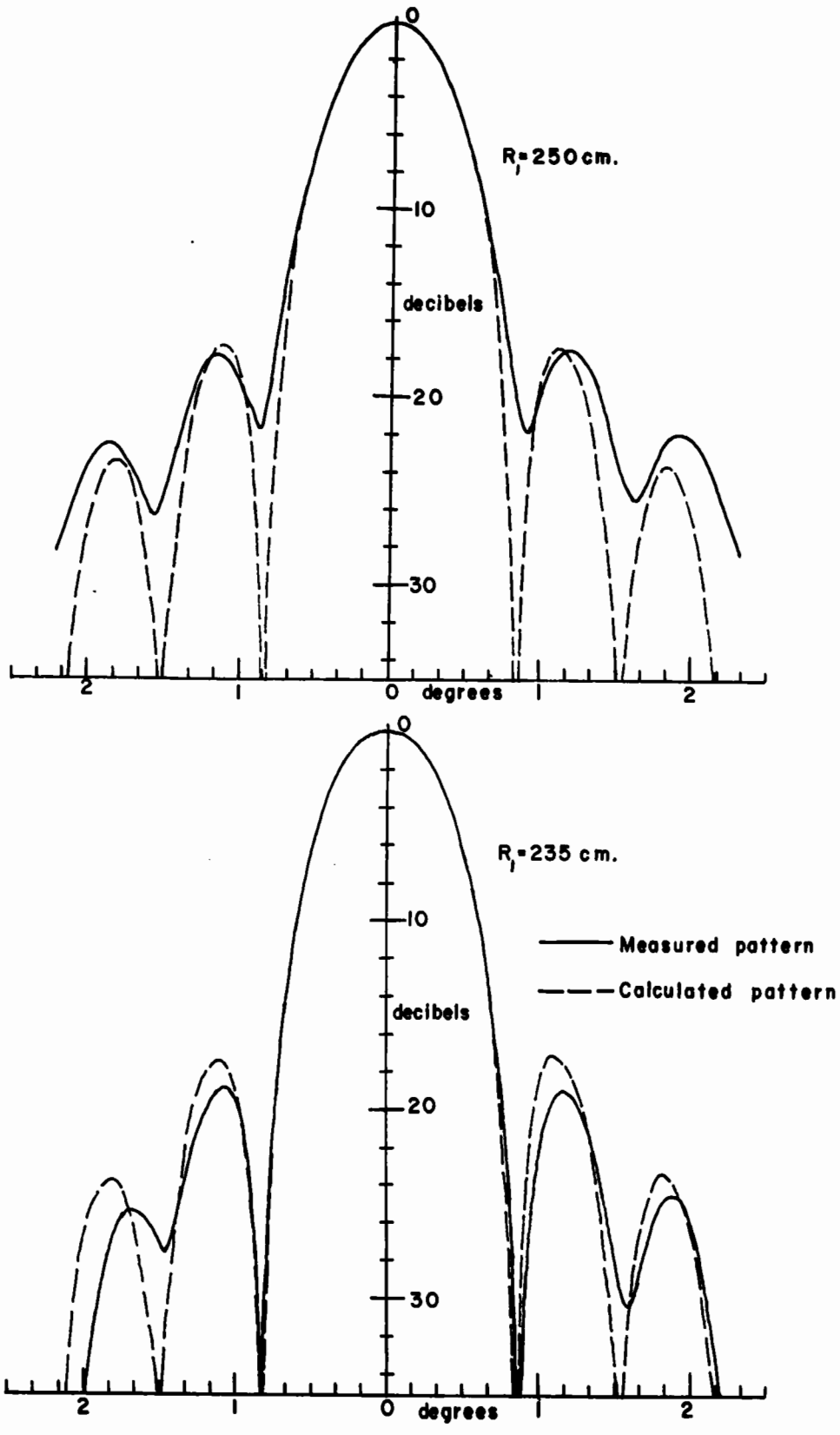

Fig. 3.4: Back-scattering patterns of a 50 cm. diameter circular disc measured using System IV.

corrected for spherical aberration. In general, other aberrations appear when the source illuminating the lens is displaced off the principal axis of the lens. These include coma, astigmatism, distortion, and curvature of field.[7, 9] Such off-axis aberrations cause a deterioration in the process of collimation performed by the lens, and appear in System IV when the lens is rotated with the antenna or scatterer. (However, it will be noted that lens C was corrected for coma as well as spherical aberration).

With a view to improving System IV, knowledge of the effect of aberrations alone on the measured antenna patterns was desired: If lens aberrations accounted for much of the inaccuracy in the patterns, improvements in the optics of System IV should lead to better results. Calculations of the true E-plane pattern of the 10λ horn are made in Appendix IV, followed by calculations for the same horn which take account of the aberrations in lens A that modify the pattern measured using System IV. The results are given in figure (3.5). It is seen that the lens aberrations should have little effect on the pattern measured using System IV for angles of rotation of the lens and horn up to about 20 degrees. It can be concluded then, that other sources of error are more serious than lens aberrations, for small angles of rotation at least.

This result is confirmed by the measurement of the back-scattering pattern of the aluminum plate. For

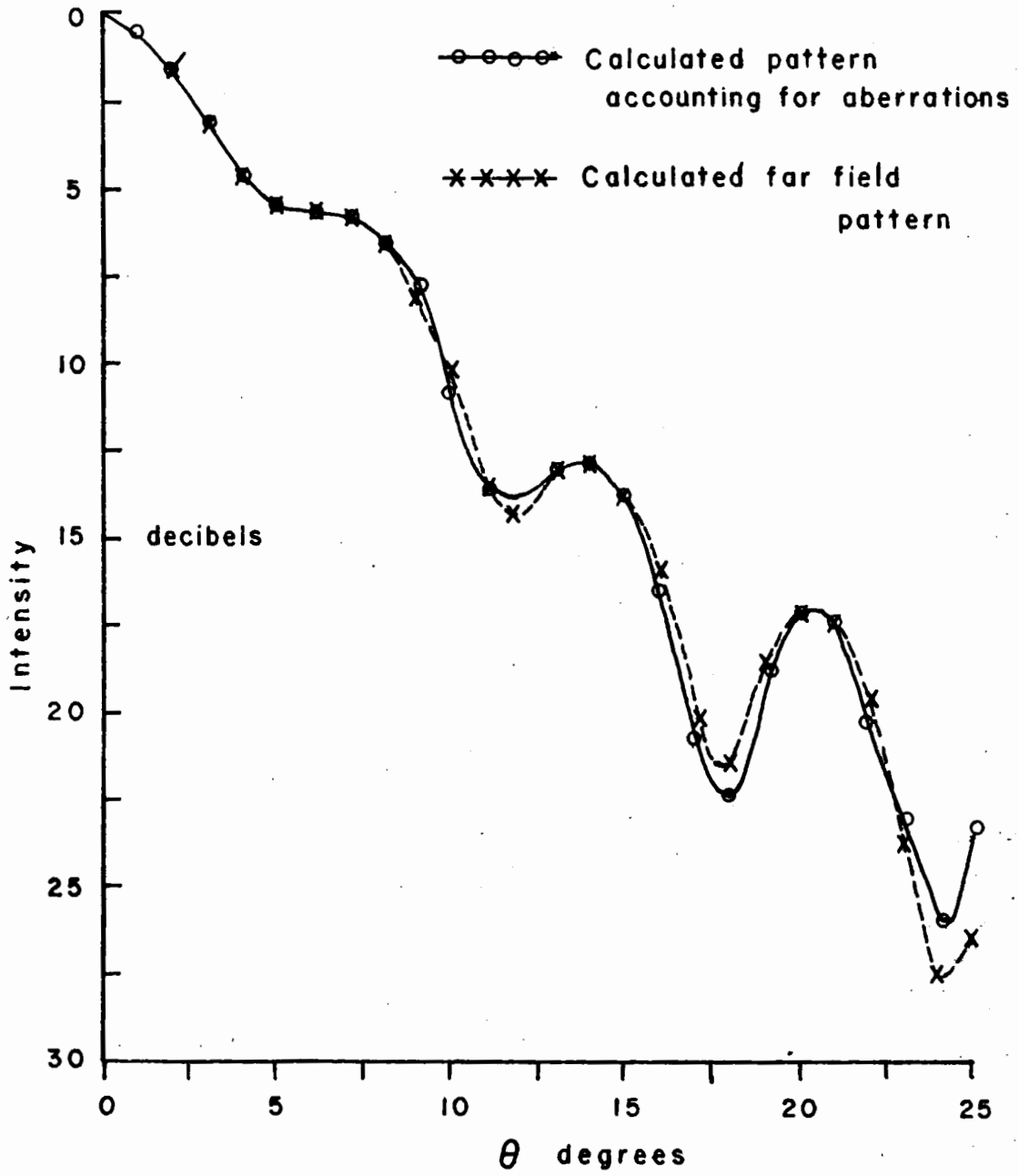

Fig. 3.5: The calculated E-plane patterns of the 10 λ horn.

the angle of rotation of about ± 2 degrees, which covered the major parts of the back-scattering pattern, lens aberrations should be negligible. Yet some departure from the ideal back-scattering pattern was found.

(b) Perturbations in the Field Emerging from the Collimating Lens: It was found in System I that the field emerging from the collimating lens had smaller variations in phase and amplitude very near the lens surface than in other regions of the collimated beam. System IV was based on this information, and improvements in the measured antenna patterns were obtained employing System IV as compared to System I. However, variations in the field near the surface of the collimating lens are still significant and undoubtedly cause some of the error found in the antenna patterns measured using System IV.

The field variations at the surface of a lens mounted in an aperture arise from a combination of two effects. The first, originally discovered by Andrews,[10] is the fluctuation of the field in the aperture of a screen, with no lens present. This fluctuation results from perturbation of the incident wave by the aperture rim (i.e., it is a diffraction effect). The second cause of field variations is the lens itself.[11] For the simplest case of a plane wave incident on an infinite sheet of dielectric, a periodic variation in transmission with sheet thickness can be easily shown to result from internal reflections between the dielectric surfaces. A similar variation in transmission might be expected over the surface of a dielectric lens,

since the thickness of the lens varies with the distance from the center of the lens.

A dielectric lens presents an electromagnetic problem of such complexity, that regardless of the manner of mounting the lens (which serves only to complicate the problem more) a theoretical solution for the field at the surface is very unlikely. For this reason, no means of reducing the field perturbation at the surface of the lens can be suggested.

(c) Multiple Reflections Between the Lens Surfaces, the Object Under Test, and the Transmitting Antenna: In antenna measurements, multiple reflections between the transmitting and receiving antennas are an inherent source of error. These reflections are particularly important in laboratory measuring systems, because their effect increases with smaller separation of the transmitter from the receiver.[1] (This dependence of reflections on the separation (R_1) may explain the slightly better results obtained using lens A compared with lens C. In System IV, R_1 was made equal to the lens focal length. This was 250 cm. for lens A, but only 100 cm. for lens C.)

Reflections also take place between the surfaces of the lens and the transmitting antenna. In the back-scattering measurements, a plano-convex lens was used (lens A) with the curved surface facing the transmitter. Reflections from this curved surface would interfere with the reflections from the plate and could lead to the filling in of the minima between the side lobes that can be seen in the back-scattering pattern

of the disc (figure (3.4)). The better results obtained at R = 235 cm. might be due to a more favourable phase relationship between the two reflected waves at that distance. (A similar improvement in horn patterns was not found as R_1 was decreased from 250 cm.)

Finally, reflections between the surfaces of the lens and the inside walls of the horns will cause errors in the measured horn patterns.

In summary, although many sources of error are present in System IV, their total effect on measured antenna or scatterer patterns is not so large as to preclude the use of this system for special measurements that do not require great precision. Also, possibilities exist for improving System IV. These include the use of lenses with larger focal lengths, so as to reduce the effects of reflection between the antenna under test, and the transmitting antenna. In general, lens aberrations can also be reduced by increasing the focal length,[12] and reflections from the surfaces of the lens could be made smaller with the use of non-reflecting coatings.[13, 14]

In the Conclusion, System IV is compared quantitatively with the other methods used to obtain a collimated wave that have been described previously. This follows a description in the next Chapter of the experimental methods used in all the work that has been mentioned.

Chapter 4.

EXPERIMENTAL METHODS AND APPARATUS

Essentially, the experimental procedures involved in the work that has been described, had the following general objectives:

(1) Measurement of the relative power transmitted (or received) in a specified direction by an antenna as function of the angle of rotation of the antenna with respect to this direction.

(2) Measurement of relative intensity in a microwave field as function of the position of the measuring probe.

(3) Measurement of relative phase in a microwave field as function of the position of the measuring probe.

The description that follows of the specific procedures employed to achieve these measurements will include details of the apparatus used.

2.1 Antenna and Scattering Pattern Measurements.

(a) Far Field Horn Pattern Measurements.

The site chosen for far field antenna measurements extended over a distance of 310 ft. between a turntable mounted on the roof of the Eaton Electronics Research Laboratory, and a parabolic reflector mounted on the roof of the Biology Building, McGill University. This distance surpassed the criteria given in figure (1.1) for the antenna separation necessary to ensure accurate far field measurements (i.e.,

$R \geq \frac{2D^2}{\lambda}$ and $R \geq \frac{2dD}{\lambda}$). In view of the fact that the transmitting and receiving patterns of an antenna are identical,[1] for convenience, the three horns whose far field patterns were desired, were used as transmitting rather than receiving antennas in these measurements.

The receiving antenna was a 30 inch diameter parabolic reflector with an open waveguide front feed. A photograph of the antenna is shown in figure (4.1a) and a general view of the receiving site in figure (4.1b). This antenna was constructed in conjunction with Mr. G. Cloutier of the Eaton Electronics Research Laboratory. Its characteristics were: a gain of over 40 decibels, half power beam width of about 1.5 degrees, and a first side lobe level more than 23 decibels below the maximum of the main lobe. This narrow beam width and low side lobe level, combined with the relatively unobstructed path between the transmitter and receiver, prevented any reflection from the ground or buildings from producing a significant response in the receiver.

The three horns used as test antennas in the work covered in previous chapters, have been described in Table I. A photograph of these horns (with a smaller rectangular horn used for lens illumination) is shown in figure (4.1c). The three horns were suitable test antennas because their construction (from sheet copper) was sufficiently rugged that their radiation characteristics remained unchanged during the many adjustments and modifi-

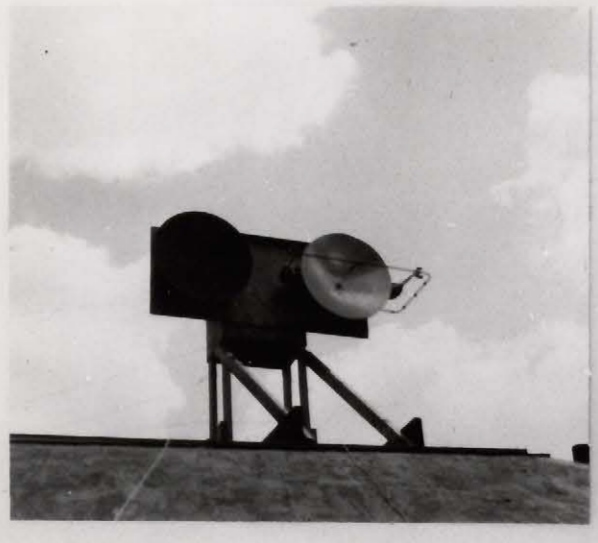

(a): (Right) The parabolic receiving antenna.

(b): A view of the receiving antenna (center) from the transmitter.

(c): From the left: the small horn used in lens illumination, and the 10, 15, and 26 λ horns.

Fig. 4.1

cations of apparatus required in the work.

The horns were mounted on a large turntable that is permanently installed on the roof of the Eaton Electronics Research Laboratory. This turntable was driven by a D.C. motor which was controlled by an amplidyne system. A synchro generator geared to the turntable, formed part of the servo-system of a rectangular co-ordinate recorder (to be described below). The horns radiated microwave power that was generated (for all measurements to be discussed) by a tunable 2K 33 klystron. For the particular klystron used, a maximum power output of about 20 milliwatts was found at a wavelength of 1.235 cm.: This wavelength was then used consistently throughout the work. A type 801 universal power supply gave klystron reflector modulation, filament voltage, and D.C. power. The A.C. supply for the equipment was stabilized with a voltage regulator. Square wave modulation was employed at a frequency of 1000 c/s.

In the measurement of the far field patterns, the klystron with accessory wavemeter and tuner, was attached to the horn, and the whole assembly mounted on the turntable at such a height as to be in the same horizontal plane as the parabolic receiving antenna. This height was determined with a transit, at the same time that the separation between the transmitter and receiver was measured. A chosen edge of the horn aperture was adjusted, with the aid of a carpenter's level, until horizontal. Then, again using the carpenter's level, the longitudinal axis of the horn was aligned so that the aperture was in a vertical plane.

Power received by the parabolic reflector was carried by waveguide from the open waveguide feed, through a tuner, to a crystal detector, and the 1000 c/s audio signal resulting from demodulation was transmitted from this crystal to a tuned amplifier. The amplifier formed part of an Airborne Instruments Laboratory Type 373 Rectangular Co-ordinate Recorder, and this equipment was located for convenience close to the klystron power supply in the Eaton Electronics Research Laboratory. The recorder had a pen movement corresponding to a 40 decibel range of microwave power, when used with a square law detector. Linearity of the recorder itself was very good, but care was necessary in selecting a crystal with voltage output proportional to power input over the full range of the recorder. Linearity of the whole system was bench checked using a calibrated precision microwave attenuator and, with a proper choice of crystal, no departure from linearity was found. An audio signal of about .5 microvolts from the crystal could be detected by the recording system, and the power levels recorded with the apparatus are estimated to be accurate to within about .25 decibels.

In taking the horn patterns, the position of the recorder pen was determined by the received power level. The pattern was inscribed by the pen on a paper chart which was positioned by a servo-system according to the angle of rotation of the turntable and horn. Thus the pattern resulting from rotation of the horn was a decibel plot of power transmitted by the horn in the direction of the

parabolic reflector, as function of the angle of rotation of the horn about this direction.

(b) Laboratory Horn Pattern Measurements.

The procedure followed when the horn patterns were measured in the various collimated fields produced in the laboratory was almost identical to that described above. The major difference was that the horns were now used as receiving antennas, with a tuner and crystal detector attached. The horns were mounted on a small turntable that could be easily moved, and this was provided with synchro generators to allow angular position to be recorded in the same manner as before.

The klystron was now used as the source of power feeding either an open waveguide radiator or a small horn antenna. Energy from these radiators illuminated the lenses used in the collimating systems discussed in Chapter 2. (The small horn antenna is seen at the left of figure (4.1c).

Some of the physical properties of the lenses themselves, have already been described in Table II. A photograph of lens A mounted in the screen is shown in figure (4.2a). Lenses A and B were designed and constructed by M.P. Bachynski,[7] and lens C by M.H. Chapman.[15] All three lenses were unstepped, and accurately machined from solid polystyrene.

The general experimental arrangements used in taking the horn patterns in the collimated beams, have been sketched in the figures of Chapter 2. The procedure used in these measurements was as follows: the turntable was

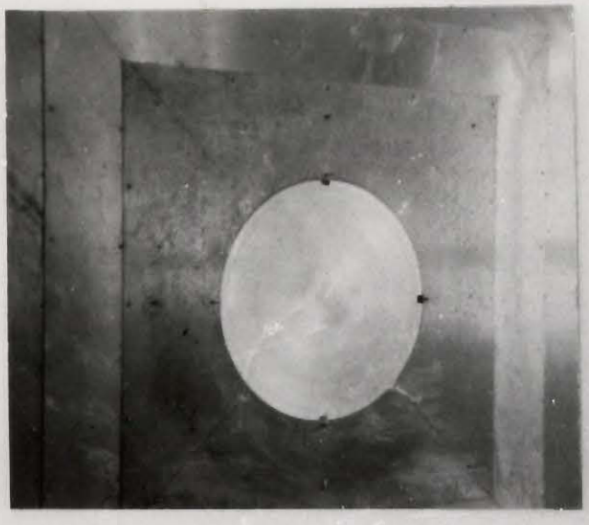

(a): LensA mounted in a metal screen

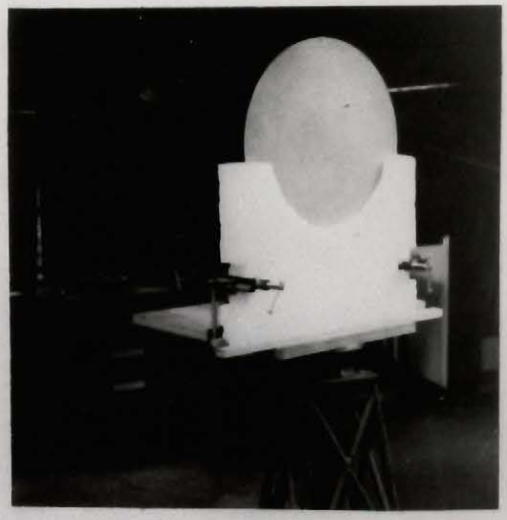

(b): Scattering plate mounted behind lens A, and supported on a small turntable.

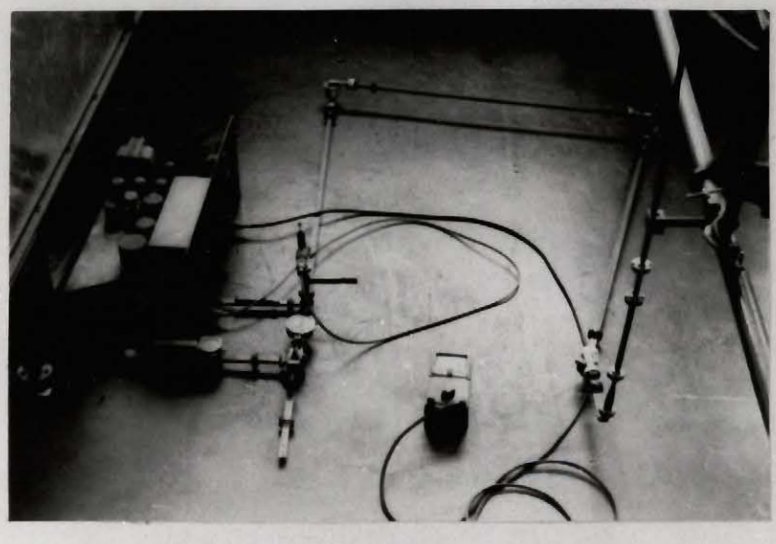

(c): Phase-measuring apparatus.

Fig. 4.2

placed along the optical axis the desired distance from the collimating lens, and levelled. Its axis of rotation was then vertical and intersected the optical axis of the system. The horn was mounted on the turntable with the center of its aperture at the point of intersection of these axes. Levelling of the horn was carried out as in the far field measurements.

A pattern of the power response of the horn as a function of its angular position in the field was provided by the recording system, once the required connections had been made for the servo-system and the audio lines leading from the crystal detector to the amplifier.

In all of the laboratory measurements, room reflections had to be reduced by careful placement of microwave absorbing material.* The absorber was particularly necessary on the image side of the metallic screen supporting the collimating lens, to minimize reflections between this screen and the horn under test. However, once the absorber had been added, smooth and symmetrical horn patterns were generally achieved, and it is believed that room reflections caused little error in these patterns.

(c) Laboratory Back-Scattering Measurements.

A schematic diagram of the back-scattering system was given in figure (2.3), and shown here, in figure (4.2b), is a photograph of the scattering plate and lens, mounted on the

---

* "Darkflex," Sponge Rubber Products, Shelton, Conn.

small turntable that was used for all laboratory pattern measurements. The plate and lens were supported by a polystyrene foam block, which had a very low index of refraction and caused negligible reflection. Reflections from the turntable, the support, and the support mounts were checked by rotating the turntable and this apparatus, without the lens or plate in place. The reflected power received as the turntable rotated was almost constant: the signal that was detected, was largely due to limited discrimination in the transmitting and receiving apparatus to be described next.

Referring to figure (4.3), the magic tee arrangement shown was used to separate the direct power generated by the klystron from the reflected power, returning from the scattering object, and received by the small horn. This arrangement is essentially the same as that used by Hogg,[4] whose optical system corresponded to System I. It is possible to match the arms of the magic tee so that, with no scatterer in position, verylittle of the direct power from the klystron reaches the crystal arm of the tee, while, when the scatterer is in place, nearly all of the reflected energy received by the horn is detected by the crystal. When this was done, it was found that the residual signal reaching the crystal, with no scatterer present, was about 40 decibels below the maximum reflected signal with the lens and scattering plate mounted on the turntable. (Much better discrimination than this is possible, but it requires

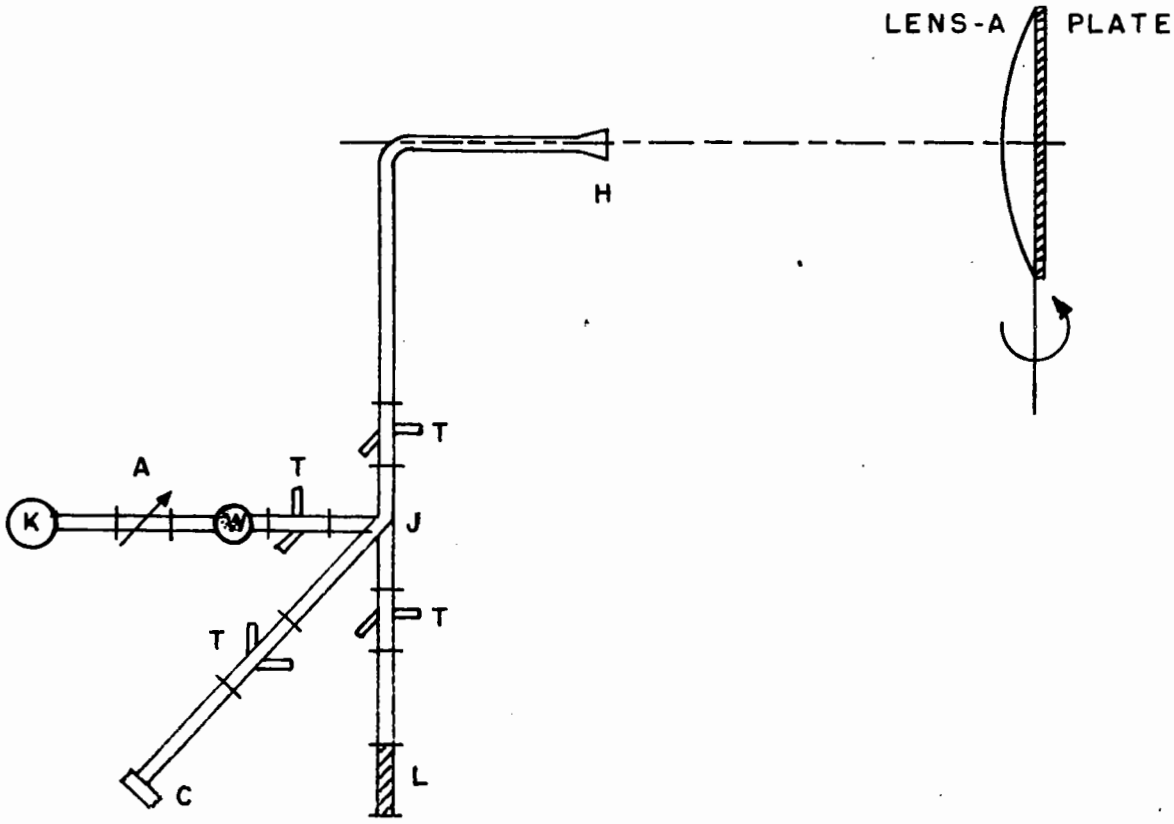

H = HORN
T = TUNER
C = CRYSTAL
K = KLYSTRON
W = WAVEMETER
L = FLAT LOAD
J = HYBRID JUNCTION (MAGIC TEE)
A = ATTENUATOR

Fig. 4.3: Schematic diagram of the back-scattering apparatus.

elaborate frequency stabilization of the source.) Thus, when the lens and plate are rotated with the turntable, the reflected power detected by the crystal is recorded to give a pattern in the same manner as previously described.

4.2 Intensity Measurements in the Collimated Beams.

Measurements of intensity in the fields produced using the four collimating systems were relatively simple. An optical bench was placed in each case parallel to the collimating lens and an open waveguide probe, supported on the bench, was moved by a worm gear. The position of the probe was again recorded through the use of a selsyn generator, which was connected to the worm gear. The worm gear itself was driven by an A.C. motor. The signal received by the probe was detected by a crystal, and the audio output from the crystal transmitted with a shielded line to the tuned amplifier of the recording system. In this way, a plot of field intensity as function of the position of the probe in the field was obtained.

4.3 Phase Measurements in the Collimated Beams.

The interference method of phase measurement[1] was used to obtain the phase plots presented in preceding chapters. This method involves the mixing of a signal sampled from the field of interest, with a reference signal of similar amplitude. The phase of the reference signal is varied so as to produce a minimum in the mixed signal output, this condition indicating that the reference and test signals are

180 degrees out of phase. By recording the phase changes in the reference signal necessary to produce this minimum output for various positions of the sampling probe, the relative phase of the field at these positions can be determined.

A schematic diagram of the system is shown in figure (4.4) and a photograph of the mixing section of the apparatus in figure (4.2c). Part of the klystron power is diverted with a magic tee into a reference path. The electrical length of this path can be varied by adjusting a slotted line, so as to change the phase of the reference signal arriving at a second magic tee. The signal sampled from the field by an open waveguide probe, passes through a waveguide section containing three rotary joints to this second tee where the two signals are combined. The rotary joints allowed movement of the probe without appreciable change in the electrical length of the waveguide between the probe and the magic tee. The combined signal is detected by a crystal in one arm of the magic tee. The output is amplified and displayed on a meter. The position of the probe, and the adjustment of the slotted line necessary to produce a minimum output are recorded by hand.

Knowing the klystron frequency, the guide wavelength is determined, and the phase shifts produced by adjustment of the slotted line calculated. These phase shifts are plotted against the position of the measuring probe to give the relative phase of the field. The system was checked using an open waveguide radiator to give a known spherical

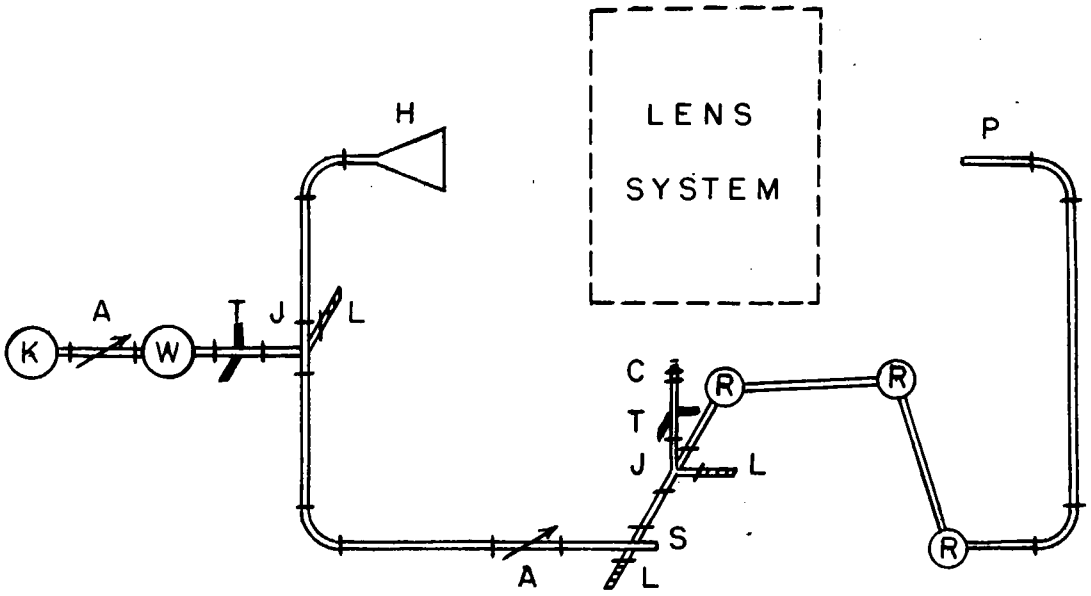

LEGEND :

P :	PROBE	J :	MAGIC TEE
K :	KLYSTRON	W :	WAVEMETER
A :	ATTENUATOR	L :	FLAT LOAD
T :	TUNER	S :	SLOTTED LINE
C :	CRYSTAL	R :	ROTARY JOINT
H :	TRANSMITTING ANTENNA		

Fig. 4.4: Schematic diagram of the phase-measuring apparatus.

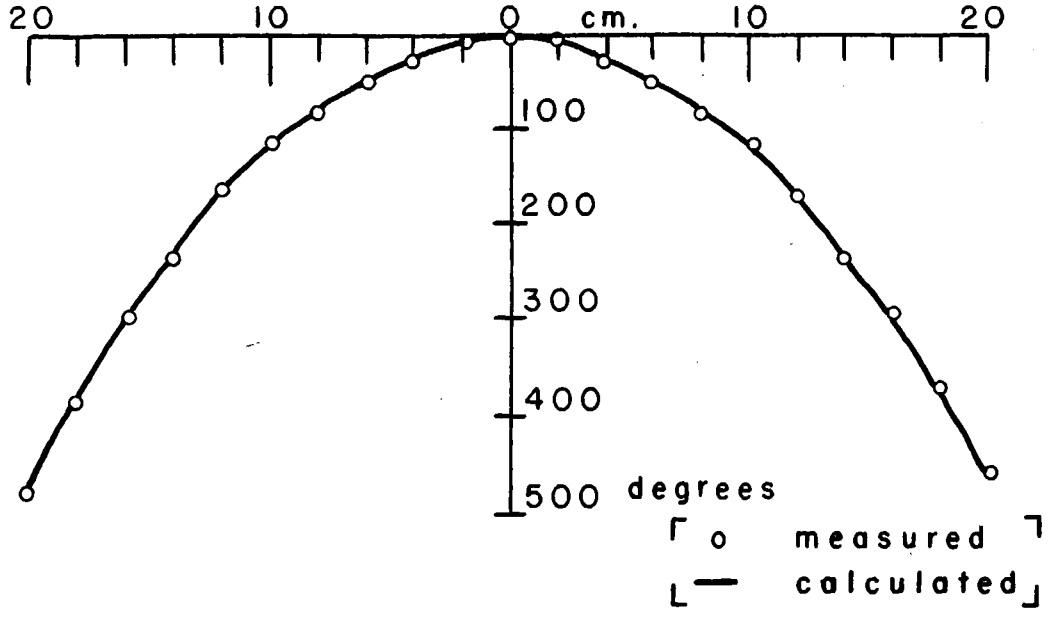

Fig. 4.5: Measured and calculated phase variation in a scan across a spherical wavefront, 122 cm. from a small source.

wavefront. Calculations were made of the changes in phase in a scan over this wavefront at a distance of 122 cm. from the source. These calculations are compared with the measured phase changes in figure (4.5), and from the results, the system was estimated to be accurate to within about 10 degrees.

Chapter 5.

CONCLUSION

A comparison will be made in this concluding chapter of the four microwave collimating systems investigated, after the main ideas involved in the work have been briefly summarized below.

In the introduction, the disadvantages of the standard far field method of antenna measurements were pointed out, while in Chapter 2 the need for some form of collimating device to produce a plane wave for laboratory antenna measurements was demonstrated: Serious inaccuracies were encountered when antenna patterns were taken in the laboratory using the spherical wave from a point source. However, in collimating this spherical wave with a lens (as in System I), difficulties arise at microwave frequencies from diffraction at the edge of the lens, which causes severe departure of the field from what would otherwise be a plane wave. It was established with System II, that these diffraction effects can be reduced by tapering the illumination falling on the collimating lens. The tapering resulted in a greatly improved amplitude distribution in the collimated beam, but the phase distribution was poor. However, by choosing a special form of amplitude taper, combined with a modified phase distribution over the collimating lens (as in System III) the phase variations, over a sizable region of the collimated field, were sharply reduced. Yet, although the amplitude was smoothly varying in this region, it was not sufficiently uniform to allow accurate measurement of

of the radiation patterns of large antennas. Finally, a simple modification of System I was tried, by means of which the best portion of the collimated field, found very close to the lens, could be used for special antenna and scattering measurements.

With reference to Table III, the results of antenna measurements using the four collimating systems will now be compared. Wherever possible, data for this table were taken from patterns presented in the thesis; these patterns were considered representative of a large number recorded during the course of the work. To give some indication of the accuracy of the E-plane pattern measurements, errors in the first and second side lobe levels are listed, while for the H-plane patterns, the errors in the full width of the main lobe 10 decibels below the maximum are given. All errors were read with the maximum of the main lobe of the pattern concerned, coinciding with the maximum of the true pattern.

For System I, large and varied inaccuracies are listed for both the E and H-plane measurements for all horns. (These data were taken from horn pattern measurements made at different distances from the lens, see figure (2.8)). An excellent E-plane pattern of the 10λ horn was obtained using System II. The small amount of phase error over the horn had more effect on the H-plane pattern measured with this system. Greater inaccuracy resulted in both E and H-plane measurements of the 15λ and 26λ horns because of the larger amounts of phase error over their apertures, but the figures indicate considerable improvement using System II as compared with System I. As

TABLE III

SYSTEM	HORN	PATTERN ERRORS					
		1st Side Lobe E-Plane (decibels)	2nd Side Lobe E-Plane (decibels)	10 db. Beam Width		Average	
				degrees	%	Lobes db	Width %
I	10 λ	2 to 6.5	2 to 9	2	13	4	39
	15 λ	2 to 3	2.5 to 4	2 to 12	18 to 109		
	26 λ	2* to 5	2.5 to 9*	4*	14*		
II	10 λ	0.3	0.4	1.5	10	1.6	13
	15 λ	1.8	1.3	2.5	23		
	26 λ	1.8	4	1.9	7		
III	10 λ	1.9	2	0.2	1.3	4	13
	15 λ	4*	7*	0.3	2.7		
	26 λ	2	7	10	36		
IV	10 λ	0.2	1.1	0.3	2	0.5	5
	15 λ	0.2	0.7	0.8	7		
	26 λ	0.3	0.4	2	7		

* FROM PATTERNS NOT SHOWN

already mentioned, with System III, inaccuracy in the antenna patterns was due to amplitude variation in the field, but this did not cause significant errors in the H-plane patterns of the 10 and 15 λ horns. The E-plane patterns were more seriously modified by this variation.

Finally, it is seen that the most consistently accurate results are obtained using System IV. Only the H-plane pattern of the 26 λ horn was poor, and the errors in this pattern are at least smaller than those found using the other three systems. Errors of the magnitude tabulated for this system, averaging about 0.5 decibels in side lobe level and 5% in beam width, could be tolerated for many antenna and scattering measurements, and the suggestions given in Chapter 3 for improving the system, would possibly increase the accuracy even more. However, measurements with the system are limited to those involving plane scatterers or antennas having a plane aperture. Moreover, if patterns extending over larger angles of rotation were desired, errors would be increased by off-axis lens aberrations, which eventually become serious.

It is believed that System III, employing the Gaussian amplitude and quadratic phase distributions over the collimating lens, shows the greatest promise for accurate laboratory measurements of a more general nature. As pointed out in Chapter 2, there is no inherent limitation on the volume of the region over which uniform phase and amplitude could be achieved with this system. Larger lenses are required to extend the amplitude distribution, but if necessity warranted, a collimated field could be produced meeting given specifications.

APPENDIX I

Diffraction Theory

In Chapter 2, equation (2.1) is stated to give a general expression for the field (u_Q) at some point Q beyond a circular aperture contained in a screen, in terms of the field in the aperture. This result is based on the scalar Kirchhoff theory of diffraction[16, 17], and the derivation is outlined below.

Although vector solutions[18, 19, 20] of the problem are available, which give a more exact representation of the electromagnetic field (particularly in and near the aperture), the use of the approximate Kirchhoff theory is justified here on the basis of experimental measurements [21] at microwave frequencies which have shown that this simpler scalar theory is adequate for distances 20 wavelengths or more from circular apertures larger than about 10 wavelengths.

By applying Green's theorem, it can be shown[16] that, for a field satisfying the scalar Helmholtz equation, $(\nabla^2 + k^2)u = 0$, the amplitude at some point Q in a source-free region beyond an infinite plane screen containing an aperture is given by:

AI.1
$$u_Q = \frac{1}{2\pi}\int_A u_A \frac{\partial}{\partial n}\left(\frac{e^{-jks}}{s}\right) dA$$

where u_A is the field over the screen and aperture, n is a unit normal directed from the screen into the region of interest, and s is the distance from the element of screen or aperture area dA to the field point Q. Kirchhoff's assumptions are: the field over the screen is zero everywhere

except in the aperture, where it is equal to the unperturbed incident field (u_i). Then the area of integration is limited to the aperture area (A_o). Performing the differentiation in equation AI.1 gives:

$$\text{AI.2} \qquad u_Q = \frac{1}{2\pi} \int_{A_o} u_i \left(-jk - \frac{1}{s}\right) \frac{e^{-jks}}{s} \cos(n,s)\, dA_o$$

For regions where the theory is valid (i.e., 20 wavelengths or more from the aperture) the second term is small compared with the first, and can be neglected. With a circular aperture, the position of the element of aperture area (dA_o) is specified by polar co-ordinates (ρ, ϕ) and Q is located in a plane parallel to the screen and some distance R_1 from the screen. The distance between Q and the axis of symmetry will be denoted by ξ, and for small values of ξ, the factor Cos (n, s) in equation AI.2 can be set equal to unity. For simplicity, ϕ is chosen to be zero in a plane containing the axis of symmetry and the ξ co-ordinate axis. Then the distance s from dA_o to Q can be written:

$$\text{AI.3} \qquad s = \left(R_1^2 + (\xi - \rho\cos\phi)^2 + (\rho \sin\phi)^2\right)^{1/2}$$
$$= \left(R^2 + \rho^2 - 2\rho\xi\cos\phi\right)^{1/2}$$

where $R = (R_1^2 + \xi^2)^{1/2}$ is the distance from the center of the aperture to the point Q.

For $R \gg \xi, \rho$, an additional approximation is made by expanding this expression for s, and retaining only the first terms, to give the result:

AI.4 $$s \doteq R + \frac{\rho^2}{2R} - \rho\frac{\xi \cos\phi}{R}$$

Putting this value of s into equation AI.2, and using the other approximations mentioned, the following expression is obtained:

AI.5 $$u_Q = \frac{-jk}{2\pi}\int_0^{2\pi} d\phi \int_0^a \rho \frac{u_i}{R} e^{-jk\left(R + \frac{\rho^2}{2R} - \rho\frac{\xi\cos\phi}{R}\right)} d\rho$$

Where (a) is the aperture radius, and s is approximated by R (or R_1) in the denominator, with little error.

Finally, if u_i, the field in the aperture, is a function of ρ alone, then the ϕ integration can be performed in equation AI.5 to give the required result:

(2.1) $$u_Q = -jk\frac{e^{-jkR}}{R}a^2\int_0^1 u_i\, r\, J_0\left(\frac{k\xi a r}{R}\right) e^{-j\frac{ka^2r^2}{2R}} dr$$

The remaining integral has been normalized by putting $\rho = ar$.

APPENDIX II

Approximate Evaluation of the Collimated Field in System II.

The expression given in Chapter 2 for the field in the collimated beam of System II was:

$$(2.6)\quad u_{QA} = -j\frac{R_1}{R_2}\frac{a}{b}u_o'\left\{ e^{-jk\left(R_o+R_1+R_2+\frac{n^2}{2R_2}\right)} \cdot\int_o^1 J_1\left(\frac{kbar}{R_1}\right) J_o\left(\frac{kan\,r}{R_2}\right) e^{-j\frac{ka^2r^2}{2R_2}}\,dr\right\}$$

An evaluation of the integral in this equation will be undertaken here using the following approximation of the function $\frac{J_1(q)}{q}$:

$$\text{AII.1}\quad \frac{J_1(q)}{q} \doteq \frac{e^{-q^2/8}}{2}\left(1-\left(\frac{q}{\phi}\right)^4\right)$$

where

$\phi = 3.8317$, is the first root of the Bessel function J_1 (i.e., $J_1(\phi) = 0$). The function on the right of equation (AII.1) is plotted in figure (A2.1) in comparison with $\frac{J_1(q)}{q}$ and it is seen that the agreement is good up to values of q slightly larger than ϕ. To further justify the use of this approximation, it should be pointed out that in the calculated illumination falling on the collimating lens of System II (i.e., $\left(\frac{J_1(q)}{q}\right)^2$), more than 83% of the energy is concentrated in the region $q \leq \phi$ (q for the experimental arrangement is given by $q = \frac{kbar}{R_1}$), and the side lobes

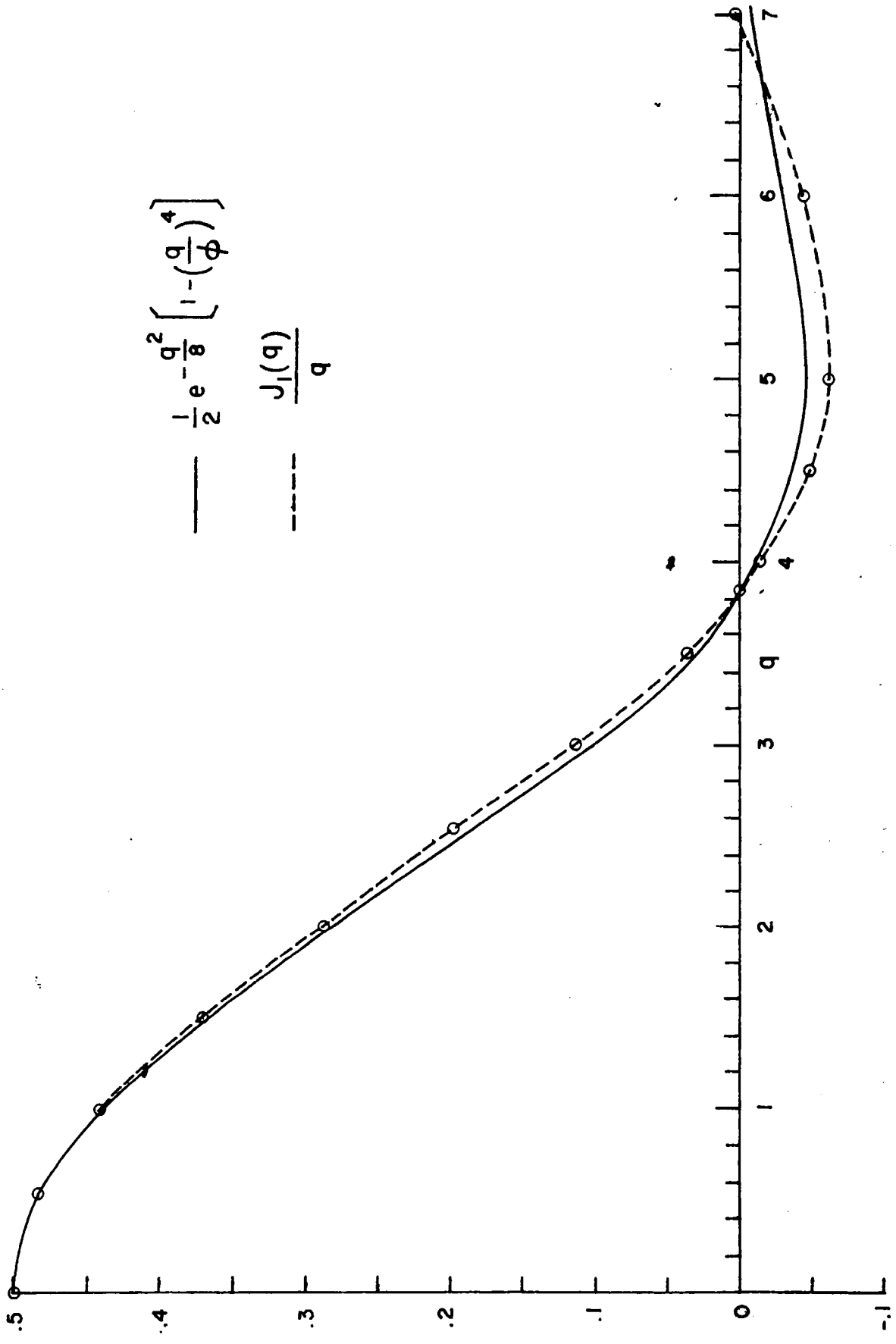
$\frac{1}{2} e^{-\frac{q^2}{8}\left[1-\left(\frac{q}{\phi}\right)^4\right]}$
$\frac{J_1(q)}{q}$
.5
.4
.3
.2
.1
0
-.1
1
2
3
q
4
5
6
7

Fig. A2.1

in the illumination beyond the first, do not contribute greatly to the field at the point Q.

Making the change of variable $ar = x$ in equation (2.6), and then letting $a \to \infty$ for reasons outlined in the text of section (2.2), the substitution of (AII.1) into equation (2.6) yields the integral:

$$u_{QA} = u e^{-j\frac{kn^2}{2R_2}} \int_0^\infty \left\{ x J_0\left(\frac{knx}{R_2}\right)\left(1 - \left(\frac{kbx}{R_1\Phi}\right)^4\right) \cdot \right.$$

$$\left. \cdot e^{-\left(\frac{kb}{2R_1}\right)^2 \frac{x^2}{2} - jk\frac{x^2}{2R_2}} dx \right\} \qquad \text{(AII.2)}$$

where u includes the constant amplitude and phase terms (only the relative values of phase and amplitude are of interest here).

By setting $\frac{kb}{R_1} = \beta$, $\frac{k}{2R_2} = \gamma$ and using the the integral representation of $J_0(\alpha x)$ given by:

$$J_0(\alpha x) = \frac{1}{2\pi j} \oint \frac{e^{t - \frac{\alpha^2 x^2}{4t}}}{t} dt$$

equation (AII.2) can be written:

$$u_{QA} = \frac{u e^{-j\frac{kn^2}{2R_2}}}{2\pi j} \oint \frac{e^t}{t} \int_0^\infty x\left(1 - \left(\frac{\beta x}{\Phi}\right)^4\right) e^{-x^2\left(j\gamma + \frac{\beta^2}{8} + \frac{\left(\frac{kn}{R_2}\right)^2}{4t}\right)} dx\, dt$$

The above expression can now be integrated to give the result shown in Chapter 2, namely:

$$(2.7)\quad u_{QA} = \frac{u}{4\left(j\gamma+\frac{\beta^2}{8}\right)}\left\{1 - 2\left(\frac{\beta}{\Phi}\right)^4\left[\left(\frac{kn}{2R_2\left(j\gamma+\frac{\beta^2}{8}\right)}\right)^4 - \frac{2k^2n^2}{R_2^2\left(j\gamma+\frac{\beta^2}{8}\right)^3}\right.\right.$$

$$\left.\left. + \frac{4}{\left(j\gamma+\frac{\beta^2}{8}\right)^2}\right]\right\}\exp\left(\frac{-jkn^2}{2R_2} + \frac{jk^2n^2\gamma}{R_2^2\left(4\gamma^2+\frac{\beta^2}{8}\right)} + \frac{\beta^2k^2n^2}{R_2^2\left(32\gamma^2+\frac{\beta^2}{2}\right)}\right)$$

Using the dimensions given for System II in figure (2.9), it was found that at a wavelength of 1.235 cm., the above expression can be simplified to give the field in the particular plane at R_2 = 200 cms., in the following form:

$$u_{QA} = Ae^{-n^2(.0047+.0122j)}\left\{(99.8 - 1.287n^2 + .0016n^4) - j(40.7 + .50n^2)\right\}$$

(n = perpendicular distance from principal axis in cm.)

From this expression, in which A is a constant, the relative phase and intensity in the plane at R_2 = 200 cm. can be readily calculated. The results have been shown in figure (2.11).

APPENDIX III

A Formula for the Evaluation of the Collimated Field of System III

The expression given in section (2.3) for the field in the collimated beam of System III was derived by considering the collimating lens infinite. For a finite lens, the field is of the following form:

$$u_{QA} = u e^{-jk\left(R_2 + \frac{n^2}{2R_2}\right)} \int_0^1 \xi' J_0(\alpha \xi')\, e^{-p\xi'^2}\, d\xi' \qquad \text{(AIII.1)}$$

where $p = \left(j\gamma_0 + j\frac{k}{2R_2} + \mu\right)a^2$, $a\xi' = \xi$ = radial distance from axis,

and $\alpha = \frac{kan}{R_2}$

the factor u includes constant amplitude and phase terms.

The integral in equation (AIII.1) can be evaluated by using a function $\delta(\xi')$ defined by:

$$\delta(\xi') = 1 \quad \text{for} \quad \xi' \leq 1$$

$$\delta(\xi') = 0 \quad \text{for} \quad \xi' > 1$$

Substituting this function into the integral of equation (AIII.1) it is seen that the limit of integration can be extended to infinity, giving the result:

$$(AIII.2)\quad u_{QA} = u e^{-jk\left(R_2 + \frac{n^2}{2R_2}\right)} \int_0^\infty \delta(\acute{\xi})\, \acute{\xi}\, J_o(\alpha \acute{\xi})\, e^{-p\acute{\xi}^2}\, d\acute{\xi}$$

If the function $\delta(\acute{\xi})$ is now represented by a Fourier-Bessel series, the integration can be performed.

$$(AIII.3)\quad \text{Let}\quad \delta(\acute{\xi}) = \sum_n C_n J_o(b_n \acute{\xi})$$

where b_n is the nth root of J_o (such that $J_o(b_n) = o$). Then it can be shown[22] that the coefficients (C_n) are given by:

$$C_n = \frac{2}{J_1^2(b_n)} \int_0^1 \delta(\acute{\xi})\, \acute{\xi}\, J_o(b_n \acute{\xi})\, d\acute{\xi}$$

$$= \frac{2}{b_n J_1(b_n)}$$

Substituting the above value of C_n into equation (AIII.3) and using this series representation of $\delta(\acute{\xi})$ in equation (AIII.2) yields the equation below:

$$u_{QA} = 2u\, e^{-jk\left(R_2 + \frac{n^2}{2R_2}\right)} \sum_n \int_0^\infty \frac{\acute{\xi}\, J_o(b_n \acute{\xi})\, J_o(\alpha \acute{\xi})}{b_n\, J_1(b_n)}\, e^{-p\acute{\xi}^2}\, d\acute{\xi}$$

$$(AIII.4)\quad = u\, e^{-jk\left(R_2 + \frac{n^2}{2R_2}\right)} \sum_n \left\{ \frac{e^{-\frac{(b_n^2 + \alpha^2)}{4p}}}{p}\, J_o\left(j\frac{\alpha b_n}{2p}\right) \right\}$$

To calculate the field in the plane at (R_2') where the infinite lens approximation indicated a uniform phase front, the value of p can be found by substituting: $-\gamma_o = \mu = \frac{k}{4R_2'}$ (the values used in section (2.3)). Then $p = \frac{ka^2}{4R_2'}(1+j)$, and the argument of the Bessel J_o in the series expansion for the field is:

$$j\frac{\alpha b_n}{2p} = \sqrt{2}\,\frac{b_n (1+j)\, n}{a}$$

Tables of J_o having this complex argument are available in Jahnke and Emde, "Tables of Functions."(23)

No numerical calculations were undertaken using equation (AIII.4) since the approximate theory derived in section (2.3) was considered adequate, in view of the fact that only an approximate Gaussian amplitude distribution was obtained experimentally. However, if a more exact Gaussian distribution were obtained, the equation should be of value in establishing theoretical criteria for the amount of taper and size of lens required to produce a specified field.

APPENDIX IV

The Effect of Aberrations in System IV

In the past, scalar Kirchhoff diffraction theory (see Appendix I) has been successfully applied to the calculation of radiation patterns of electromagnetic horns.[24] The method will be used here, to determine the effect of lens aberrations on the E-plane pattern of the 10 λ horn that was measured using System IV.

The essential idea involves the calculation of the intensity in the throat of a horn when an arbitrary wave is incident on the horn's aperture. The changes in intensity at the throat are calculated for different angles of rotation of the horn in the incident field: this gives the relative response of the horn to this field as function of the angle of rotation. It has been found that for the E-plane patterns of a radiating horn,[24] the field over the aperture appears to be that of a point source located at the horn's throat, so that the E-plane pattern is essentially the same as the diffraction pattern of an aperture (identical to the horn aperture) illuminated by a point source. With this brief outline, the equation for E-plane radiation pattern of a horn will be stated here, rather than derived, since the general method of solution is readily available in the reference given.

A rectangular co-ordinate system (x, y), is set up over the aperture of a horn, with origin on the horn's longitudinal axis, and the co-ordinates x and y in the E and H-planes

of polarization respectively. With an incident field $u_i(x, y)$ over the aperture of the horn, and an angle Θ in the E-plane between the direction of propogation of the incident field and the longitudinal axis of the horn, the amplitude at the throat of the horn is proportional to $f(\Theta)$, where this function is given by:

$$(AIV.1) \quad f(\Theta) = (1 + \cos\Theta) \int_{-\frac{b}{2}}^{\frac{b}{2}} dx \int_{-\frac{b}{2}}^{\frac{b}{2}} dy \; u_i(x,y) \cos\left(\frac{\pi y}{b}\right) e^{-jk\left(\frac{x^2}{2L_E} + \frac{y^2}{2L_H} - x\sin\Theta\right)}$$

In this equation, b is the side dimension (12.5 cm.) of the 10λ horn's square aperture, and L_E and L_H are the horn slant lengths in the two polarization planes, defined in the diagram given with Table II. The factor $\cos\left(\frac{\pi y}{b}\right)$ occurs if the TE_{01} mode is propogated in the horn, as is the case here.

When the horn is mounted behind a lens as in System IV, the effect of aberrations can be taken into account by writing the incident field u_i as:

$$(AIV.2) \quad u_i = u_o e^{-jk\,V(x,y)}$$

where u_o is a constant, and V is the aberration function[7, 12] of the lens: kV gives the difference of phase (in radians) between the actual wave emerging from the lens at a point (x, y), and the plane wave that would emerge in the absence of aberrations. The Seidel aberrations contributing to V are tabulated below.

These terms are taken from general formulas given in references (7) and (12).

(1) Coma: $\frac{n \sin\theta\,(x^2+y^2)x}{2f(n-1)} - \frac{a^3 n \sin\theta\, x}{3f^2(n-1)}$

(2) Astigmatism: $(x^2-y^2)\,\frac{\sin^2\theta}{2f}$

(3) Curvature of field and distortion: $\frac{(n+1)(x^2+y^2)\sin^2\theta}{4nf}$

(4) Spherical aberration: Since the lens was corrected for apherical aberration (lens A), this contribution to V is assumed to be zero.

In these functions, n is the refractive index of the lens (1.579), f the focal length (250 cm.), a, the radius of the lens (25 cm.), and θ the angle of displacement of the source from the principal axis (that is, the angle of rotation of the lens and horn in the E-plane).

The positive coma term in mixed x and y makes the integration in equation (AIV.1) extremely difficult. However, this term is small compared with the negative coma contribution

involving x alone. It is found by substituting the extreme values $x = y = \frac{b}{2}$ into the expression for coma, that the positive term in this expression is always less than 1/5 of the negative term. To allow integration, the positive term was neglected, so that slightly more coma was accounted for than actually existed in the lens. Adding the remaining contributions together yields the following aberration function.

$$V = \frac{\sin^2\theta}{4nf}\left(x^2(3n+1) - y^2(n-1)\right) - \left(\frac{n}{n-1}\right)\frac{a^2}{3f^2}\cdot x \sin\theta \qquad \text{(AIV.3)}$$

Substituting this value of V into equation (AIV.2) and using the incident field so obtained in equation (AIV.1), gives the result:

$$f(\theta) = \left\{ u_0(1+\cos\theta)\int_{-\frac{b}{2}}^{\frac{b}{2}} dy \cos\left(\frac{\pi y}{b}\right) e^{+jk\left(\frac{y^2}{2L_H} + y^2\sin^2\theta\left(\frac{n-1}{4nf}\right)\right)} \cdot \right.$$

$$\left. \cdot \int_{-\frac{b}{2}}^{\frac{b}{2}} dx\, e^{jk\left(\frac{x^2}{2L_E} - \frac{\sin^2\theta}{4nf}(3n+1)x^2 - x\sin\theta\left(1 - \frac{na^2}{3f^2(n-1)}\right)\right)} \right\} \qquad \text{(AIV.4)}$$

The value of the 'y' integral has very little dependence on the angle of rotation θ. Several calculations were made for specific angles, and variations of only a few percent were found (e.g., at 20 degrees, the value of the 'y' integral differs from that at zero degrees by only 1.2%).

For this reason, the calculation was greatly simplified by assuming the factor constant.

The following substitutions were made to simplify equation (AIV.4):

$$\text{Let } \frac{1}{L} = \frac{1}{L_E} - \frac{3n+1}{2n}\frac{\sin^2\theta}{f}$$

$$\text{and } \quad m = 1 - \frac{a^2 n}{3(n-1)f^2}$$

The 'x' integral of equation (AIV.4) was next transformed into a standard Fresnel integral, namely:

$$\text{(AIV.5)} \quad f(\theta) = C(1+\cos\theta)\sqrt{L}\, e^{-jkL\frac{(m\sin\theta)^2}{2}} \int_{-u_1}^{u_2} e^{j\frac{\pi s^2}{2}}\, ds$$

in which C is a constant, s a dummy variable, and u_1, u_2 are given by:

$$u_1 = \sqrt{\frac{2}{L\lambda}}\left(\frac{b}{2} - mL\sin\theta\right)$$

$$u_2 = \sqrt{\frac{2}{L\lambda}}\left(\frac{b}{2} + mL\sin\theta\right)$$

The values of $f(\theta)$ were found using a table of Fresnel integrals, and $|f(\theta)|^2$ was plotted to give the 10λ horn E-plane pattern in the presence of the aberrations of lens A as used in System IV. A similar calculation with V = o, gave the true far field pattern for comparison. The results have been shown in figure (3.5).

Bibliography

1. Silver, S., "Microwave Antenna Theory and Design," McGraw-Hill Book Co., New York (1949).

2. Woonton, G.A., Borts, R.B., and Carruthers, J.A., J.A.P., 21, 428, (1950).

3. Crysdale, J.H., "An Optical System for Antenna Measurements at Microwave Frequencies," M.Sc. Thesis, McGill University, (1953).

4. Hogg, D.C., "An Indoor Method for Measurement of Back-Scattering Coefficients," Ph.D. Thesis, McGill University, (1953).

5. Woonton, G.A., Carruthers, J.A., Elliot, A.J., and Rigby, E.G., J.A.P., 22, 390, (1950).

6. McCormick, G.C., "An Aberration Due to the Limited Aperture of a Microwave Optical System," Ph.D. Thesis, McGill University, (1953).

7. Bachynski, M.P., "Aberrations in Microwave Lenses," Ph.D. Thesis, McGill University, (1955).

8. Kerr, D.E., "Propogation of Short Radio Waves," McGraw-Hill Book Co., New York, (1951).

9. Nijboer, B.R.A., Physica, 10, 679, (1943); 13, 605, (1947); 14, 590, (1949).

10. Andrews, C.L., J.A.P., 21, 761, (1950).

11. Hogg, D.C., (Letter to the editor), J.A.P., 25, (1954).

12. Hopkins, H.H., "Wave Theory of Aberrations," Oxford University Press, London, (1950).

13. Brown, J., "Microwave Lenses," Methuen and Co., London, (1953).

14. Jones, E.M.T., and Cohn, S.B., J.A.P., 26, 252, (1955).

15. Chapman, M.H., "Design and Experimental Investigation of a Radio Lens," M.Sc. Thesis, McGill University, (1951).

16. Baker, B.B., and Copson, E.T., "The Mathematical Theory of Huygen's Principle," Oxford University Press, London, (1940).

17. Boukamp, C.J., "Diffraction Theory, a Critique of Some Recent Developments," New York University Mathematics Research Group, Report No. EM-50, (1953).

18. Stratton, J.A., and Chu, L.J., Phys. Rev., 56, 99, (1939).

19. Woonton, G.A., J.A.P., 23, 1405, (1952).

20. Bekefi, G., J.A.P., 24, 1123, (1953).

21. Bekefi, G., and Woonton, G.A., Eaton Electronics Research Laboratory, Report No. B7, (1952).

22. Tranter, C.J., "Integral Transforms in Mathematical Physics," Methuen and Co. Ltd., London, (1951).

23. Janhnke, E., and Emde, F., "Tables of Functions," Dover Publications, New York, (1945).

24. Woonton, G.A., and Tilloston, J.G., Canadian Journal of Research, A, 25, 315, (1947).